JOURNAL OF GEOPHYSICAL RESEARCH, VOL. 106, NO. D20, PAGES 24,407–24,427, OCTOBER 27, 2001

HO_x budgets in a deciduous forest: Results from the PROPHET summer 1998 campaign

D. Tan,[1,2] I. Faloona,[1,3] J. B. Simpas,[1] W. Brune,[1] P. B. Shepson,[4] T. L. Couch,[4] A. L. Sumner,[4] M. A. Carroll,[5] T. Thornberry,[5] E. Apel,[6] D. Riemer,[6,7] and W. Stockwell[8]

Abstract. Results from a tightly constrained photochemical point model for OH and HO_2 are compared to OH and HO_2 data collected during the Program for Research on Oxidants: Photochemistry, Emissions, and Transport (PROPHET) summer 1998 intensive campaign held in northern Michigan. The PROPHET campaign was located in a deciduous forest marked by relatively low NO_x levels and high isoprene emissions. Detailed HO_x budgets are presented. The model is generally unable to match the measured OH, with the observations 2.7 times greater than the model on average. The model HO_2, however, is in good agreement with the measured HO_2. Even with an additional postulated OH source from the ozonolysis of unmeasured terpenes, the measured OH is 1.5 times greater than the model; the model HO_2 with this added source is 15% to 30% higher than the measured HO_2. Moreover, the HO_2/OH ratios as modeled are 2.5 to 4 times higher than the measured ratios, indicating that the cycling between OH and HO_2 is poorly described by the model. We discuss possible reasons for the discrepancies.

1. Introduction

It has long been known that the hydroxyl radical OH and the associated hydroperoxyl radical HO_2, collectively known as HO_x, play critical roles in atmospheric oxidation [*Levy,* 1972; *Logan,* 1981]. OH is the primary atmospheric oxidant, and HO_2 is an important OH reservoir and ozone (O_3) precursor. HO_x is intimately involved in ozone production, acid rain, and particle formation. For these reasons, considerable effort has gone into attempting to understand the HO_x system. It has been only relatively recently, however, that measurements of OH and HO_2 have become available to validate the models. A few ground-based measurement campaigns, including measurements of both OH and HO_2, exist in the literature.

The Tropospheric OH Photochemistry Experiment (TOHPE) took place in the Colorado Rocky Mountains in 1993 [*Mount and Williams,* 1997]. OH was measured both by long-path absorption and by ion-assisted mass spectrometry [*Mount and Williams,* 1997, *Tanner et al.,* 1997]; both measurements were in good general agreement. HO_2 was measured by the FAGE (fluorescent assay by gas expansion) technique [*Hard et al.,* 1984, *Stevens et al.,* 1994]. A full suite of species important to HO_x were also measured, including NO_x (= NO + NO_2), NO_y (= NO_x + HONO + HNO_3 + ...), HCHO, O_3, CO, total RO_2, water vapor, nonmethane hydrocarbons (NMHC), PAN, SO_2, and the photolysis frequencies of $O_3 \rightarrow O^1D$ ($j(O^1D)$) and of $NO_2 \rightarrow$ NO ($j(NO_2)$). The model predictions for HO_x were generally higher than the measured concentrations: model OH was typically 50% higher than the measured OH [*McKeen et al.,* 1997], and model HO_2 was greater than the measured HO_2 by a factor of 3 in midday hours [*Cantrell et al.,* 1997].

The Los Angeles Free Radical Experiment (LAFRE) took place in Claremont, California, in the Los Angeles basin 55 km downwind of Los Angeles, in September 1993 [*George et al.,* 1999]. The air here is dominated by strong anthropogenic emissions. OH and HO_2 were measured by the FAGE technique. A full suite of supporting measurements were also performed, includ-

[1]Department of Meteorology, The Pennsylvania State University, University Park, Pennsylvania.

[2]Now at School of Earth and Atmospheric Sciences, Georgia Institute of Technology, Atlanta, Georgia.

[3]Now at National Center for Atmospheric Research, Boulder, Colorado.

[4]Department of Chemistry, Purdue University, West Lafayette, Indiana.

[5]Atmospheric, Oceanic, and Space Sciences, The University of Michigan, Ann Arbor, Michigan.

[6]Atmospheric Chemistry Division, National Center for Atmospheric Research, Boulder, Colorado.

[7]Now at Rosenstiel School of Marine and Atmospheric Science, The University of Miami, Miami, Florida.

[8]Desert Research Institute, Reno, Nevada.

Copyright 2001 by the American Geophysical Union.

Paper number 2001JD900016.
0148-0227/01/2001JD900016$09.00

ing NO_x, NO_y, O_3, CO, NMHC, HCHO, water vapor, $j(O^1D)$, and $j(NO_2)$. Model results for both OH and HO_2 were higher than measured OH and HO_2 in the middle of the day but agreed quite well with the measurements early in the morning and in the evening. Using the measured HO_2 as input into the model led to excellent agreement between model and measurement for OH.

The Eastern Atlantic Summer Experiment (EASE96) took place at Mace Head, Ireland, in the summer of 1996 [*Carslaw et al.*, 1999a]. The prevailing flow is westerly; the air is clean, with few fresh anthropogenic emissions, but with trace gases of marine origin, including methyl iodide (CH_3I) and dimethyl sulfide (DMS). OH and HO_2 were measured by the FAGE technique; other measurements included NO_x, NO_y, O_3, HCHO, total RO_2, total peroxides, CO, water vapor, NO_3, HONO, HNO_3, SO_2, NMHC, $j(O^1D)$, and $j(NO_2)$. The model used was a very comprehensive one, the University of Leeds Master Chemical Mechanism with 1666 reactions [*Carslaw et al.*, 1999b]: the results for OH were about 40% higher than the measured concentrations. Model HO_2 was also typically higher than measured HO_2, although there is considerable variability here.

This work presents OH and HO_2 data from the Program for Research on Oxidants: Photochemistry, Emissions, and Transport (PROPHET) summer 1998 intensive. PROPHET 1998 took place in a forested site in northern Michigan; the air is characterized by high levels of isoprene and other biogenic volatile organic compounds (BVOC) and low levels of NO. A comprehensive range of species important to HO_x were also measured, including NO, NO_2, HCHO, O_3, CO, water vapor, SO_2, alkyl and peroxyacyl nitrates, NMHC, isoprene, methacrolein, methyl vinyl ketone (MVK), 3-methyl furan, acetone, C2 - C4 aldehydes, and several monoterpenes, including α- and β-pinenes [*Carroll et al.*, this issue].

2. Experimental Details

The PROPHET site is located in the northernmost part of Michigan's lower peninsula, at 45.6° N. latitude and -84.7° W longitude. The climatology of the area is described in *Cooper et al.*, [this issue]. The site is in a hardwood forest, mostly of aspen, beech, birch, oak, and maple, with stands of Eastern white pine. Most of the measurements are drawn from a sampling manifold, whose intake is at 35 m above the forest floor, atop a 31 m permanent tower, and about 10 m above the forest canopy. Most of the instruments are located in a small laboratory at the base of the tower.

The HO_x instrument is a ground-based adaptation of the ATHOS instrument which had flown on the NASA SUCCESS and SONEX missions and has been described elsewhere [*Brune et al.*, 1998]. In essence, air is drawn through a small sampling orifice (Figure 1) by means of a Roots blower and vacuum pump to bring the pressure down from ambient to about 4 mbar. The airflow passes through a multipass White cell (typically 32-40 passes), where the sample flow is excited at a right angle to the flow by 308 nm light, which selectively excites OH radicals along the $A^2\Sigma - X^2\Pi, v' = 0 \leftarrow v'' = 0$ transition; the excited OH molecules relax at the same frequency, and this fluorescence is collected on a time-gated microchannel plate (Hamamatsu, Bridgewater, New Jersey). The reduction in pressure extends the fluorescence lifetime, allowing for efficient collection of the fluorescence signal. Pure NO is then added to the airflow to convert quantitatively HO_2 to OH. The NO concentration within the instrument is typically 1000 ppmv. NO also converts ambient RO_2 to RO, which can then react with O_2 to form HO_2, or with NO to form RONO. The latter reaction is quite fast, and under the conditions found in the White cell, competitive with the former: the HO_2 interference from 500 parts-per-trillion-by-volume (pptv) CH_3OO is calculated to be no more than 5%. From intramolecular vibrational redistribution arguments the interference from larger RO_2 should be even less. Large RO ($\geq$ C3) may also undergo isomerization and decomposition. Some of the decomposition products may lead to HO_x, after reaction with O_2 and NO: the magnitude of this interference is unknown and presently under investigation, but it is expected to be small. Total OH is detected in a second White cell, and HO_2 is determined by difference. The UV light was generated by a frequency-doubled dye laser (a heavily modified version of an old Chromatix design) using Pyrrhomethene 597 in 2-propanol and pumped by a frequency-doubled diode-pumped YAG laser from Lightwave Electronics (Mountain View, California, model 210G) operated at 3 kHz pulse repetition frequency. The UV linewidth is ~3 GHz, approximately the same as the Doppler linewidth of the OH transition. Because HO_x is so reactive and easily lost, the sample inlet and White cells had to be located atop the tower; for reasons of stability and reliability, the laser and data acquisition electronics were located in the laboratory building below. Thus the UV light had to be conveyed from the laser to the detection cells via a 0.365 mm diameter, 41 m optical fiber (ThorLabs, Newton, New Jersey). Data are collected continuously with 20 s time resolution. However, optical fiber is quite lossy at 308 nm, neccessitating a 30 min average of the 20 s data points to achieve acceptable limits of detection, which is typically better than 0.010 pptv for OH and 0.050 pptv for HO_2 in 30 min.

The instrument was calibrated before, several times during, and after the measurement campaign. The instrumental sensitivity remained essentially unchanged throughout the intensive. The water photolysis technique for generating OH was used to calibrate the instrument: 184.9 nm light from a mercury vapor lamp was used to photolyze water in a measured flow of humidified zero air just before the inlet of the instrument. Both the flow and the level of humidification (as mea-

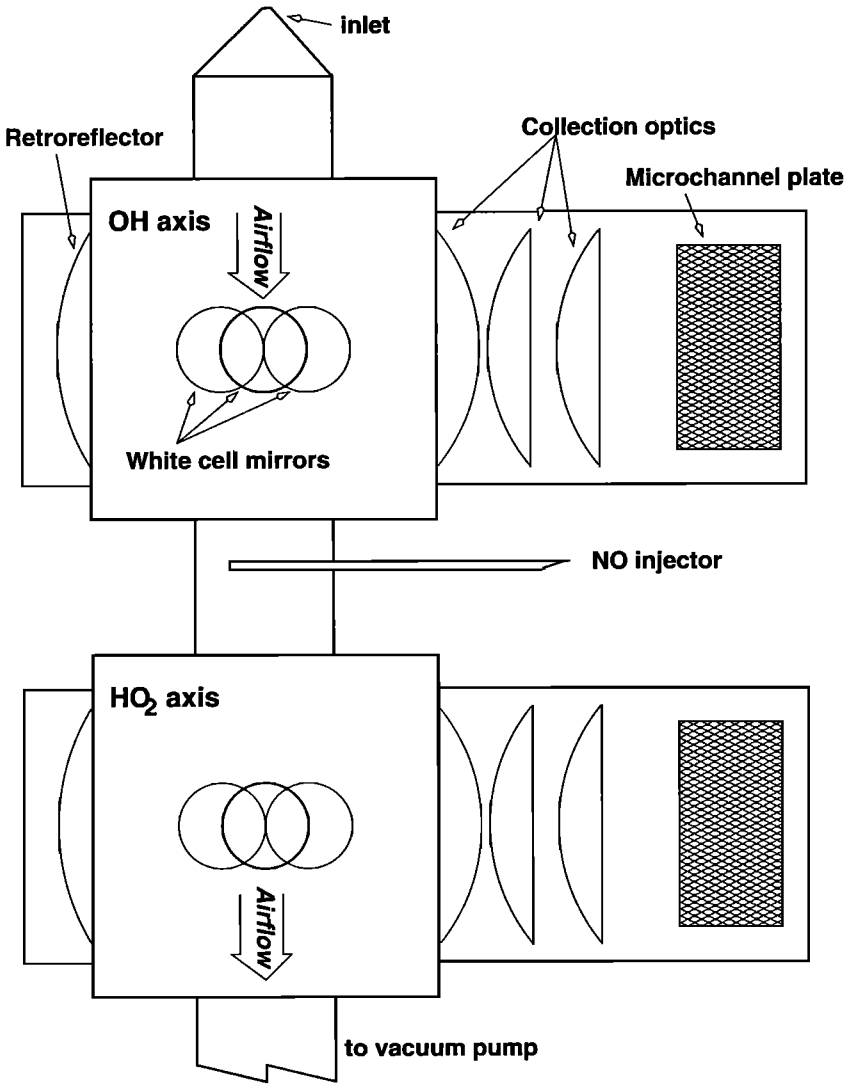

Figure 1. Schematic of the detection cells atop the PROPHET tower is shown. Ambient air is drawn through a 0.042 inch inlet past two White cells (the axis of the White cells is normal to the plane of the drawing). OH is detected in the first (top) White cell by time - gated detection of the resonance fluorescence. NO is injected into the airflow just before the second White cell to convert quantitatively HO_2 to OH. The total OH is measured in the second White cell and HO_2 determined by difference.

sured by a Licor LI6960 H_2O analyzer) were adjustable. Zero checks (with the flow on and the lamp off) ensured that no ambient air was sampled during the calibrations. The uncertainty of the instrument is estimated at ±40%, with the major uncertainty arising from the mapping of the UV flux field in the irradiation volume. The instrument was also operated with the NO off (and on at least one occasion disconnected) to ensure that there was no leakage from the NO system that could affect the OH measurement. Further details of the calibration process may be found in the work of *Faloona et al.*, [this issue].

Table 1 lists the species relevant to HO_x and the measurement techniques used during the PROPHET 1998 intensive. NO and NO_2 (converted photolytically to NO) were measured by chemiluminescence. NO_y was catalytically converted on 24 K gold (with CO added as a reductant) to NO, which was then measured by chemiluminescence [*Thornberry et al.*, this issue]. The same University of Michigan group measured CO using a TECO 48C instrument and ozone using a TECO 49C instrument.

Isoprene and its first generation oxidation products methacrolein and methyl vinyl ketone (MVK) were measured by the Purdue and National Center for Atmospheric Research (NCAR) groups using gas chromatography for separation and mass spectrometry (GC/MS) for identification. The Purdue group also measured the first generation isoprene oxidation product 3-methyl furan, as well as acetone, acetaldehyde, and propionalde-

Table 1. Measured Species Important to HO_x, Along With Measurement Techniques and Institutions Responsible for the Measurements

Species	Technique	Comment
Pressure		University of Michigan
Temperature		University of Michigan
O_3	TECO 49C	University of Michigan
NO	chemiluminescence	University of Michigan
NO_2	chemiluminescence	University of Michigan
NO_y	chemiluminescence	University of Michigan
CO	TECO 48C	University of Michigan
H_2O		University of Michigan
HCHO	fluorescence assay	Purdue University
Acetaldehyde	GC/MS	Purdue University
Acetone	GC/MS	Purdue University
Isoprene	GC/MS	Purdue University
3-methylfuran	GC/MS	Purdue University
Methacrolein	GC/MS	NCAR
MVK	GC/MS	NCAR
Toluene	GC/MS	NCAR
α-pinene	GC/MS	NCAR
β-pinene	GC/MS	NCAR
Camphene	GC/MS	NCAR
Δ^3-carene	GC/MS	NCAR
Limonene	GC/MS	NCAR
Myrcene	GC/MS	NCAR
α-phellandrene	GC/MS	NCAR
γ-terpinene	GC/MS	NCAR
PAN	GC/MS	Western Michigan University
MPAN	GC/MS	Western Michigan University
SO_2	GC/MS	Western Michigan University
Aerosol size	TSI counter	University of Michigan, Michigan Tech

hyde. The Purdue measurement drew air from the manifold for 5 min per sample onto a Tenax TA adsorbant held at 283 K. The sample is then thermally desorbed at 525 K into a Poraplot column and measured by mass spectrometry. The limit of detection for isoprene is 16 pptv in 40 min [*Barket et al.*, this issue].

NCAR measured acetone, C2-C4 aldehydes, and the monoterpenes α-pinene, β-pinene, camphene, Δ^3-carene, 1,8-cineol, limonene, myrcene, α-phellandrene, γ-terpinene, and tricyclene, as well as isoprene, methacrolein, and MVK. Three minute samples were drawn from the manifold and dried in a Silcosteel tube maintained at 263 K. The sample was concentrated in a 130 K glass bead trap, then injected into an HP-624 capillary column and measured by electron impact mass spectrometry. The limit of detection is estimated at 1 pptv.

The Purdue group measured formaldehyde by the Hantszch reaction followed by fluorescence assay: gas phase formaldehyde was extracted into purified water by means of a Nafion membrane diffusion scrubber, then reacted with NH_4^+ and 1,3-cyclohexanedione. The reaction product is illuminated with 390 nm light and the fluorescence detected. Automated 1 min injections were made every 10 min, with gas phase calibration every 2 hours. The instrumental accuracy is estimated to be $\pm 15\%$, with a 3 σ detection limit of 250 ppt [*Sumner et al.*, this issue].

3. Model

In principle, HO_x should be a very simple system to model. It responds very quickly to its photochemical environment, keeping complications from transport and mixing to a minimum. HO_x does, however, react with nearly every trace chemical species in the atmosphere, requiring reliable measurements of all of the species and photolysis frequencies important to HO_x to provide a stringent test for our understanding. A simple schematic of the reactions important to HO_x is shown in Figure 2. The mechanism for the steady-state 0-d (point) model used here draws heavily from the Regional Atmospheric Chemistry Model (RACM) [*Stockwell*, 1997]. It has been simplified significantly: for example, no NO_3 reactions or reactions involving >C3 alkanes were included. In addition, the large number of measured species precluded the need to calculate species such as formaldehyde, methyl vinyl ketone, methacrolein, etc., greatly simplifying the calculations. The model was supplemented by detailed isoprene oxidation (including isoprene-OO + isoprene-OO reactions) from *Jenkin et al.*, [1998] and *Zimmerman*

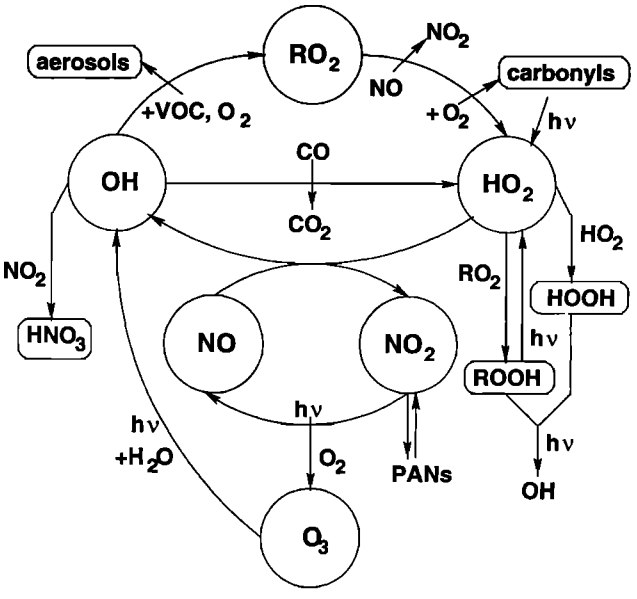

Figure 2. Schematic of the photochemistry at PROPHET.

and Poppe, [1996], by terpene ozonolysis from *Atkinson,* [1997], and by *Makar et al.,* [1999]. Tables 2-4 list the nomenclature and chemical mechanism used in the model.

A major shortcoming of the otherwise excellent measurement coverage during the PROPHET 1998 campaign was the lack of measured photolysis frequencies. An Eppley radiometer was available on the tower and was used to calculate $j(NO_2)$, using the algorithm from *Madronich,* [1987a]. There was also a Yankee UV-B radiometer at a U.S. Department of Agriculture site some 3 km from the PROPHET tower. Photolysis frequencies for $j(O^1D)$, $j(HNO_3)$, and radical and molecular channels of formaldehyde were calculated using the Madronich algorithm [*Madronich,* 1987b] and an average of the TOMS- and GOME-derived ozone columns for the PROPHET site, then scaled to a calculated fit against the measured response of the UV-B radiometer. Photolysis frequencies for peroxides, peroxynitric acid (HO_2NO_2, or PNA), higher aldehydes and ketones, and

Table 2. Species Names as Used in the Model, Along with Common Names or Chemical Formulas

Species	Comment	Name/Structure
OH	calculated	
HO_2	calculated	
MO2	calculated	CH_3OO
ACO3	calculated	CH_3CO_3
ISP1	calculated	$OOCH_2CH(OH)C(CH_3)CH_2$
ISP2	calculated	$HOCH_2CH(OO)C(CH_3)CH_2$
ISP3	calculated	$HOCH_2CHC(CH_3)CH_2OO$
ISP4	calculated	$CH_2CHC(CH_3)(COO)CH_2OO$
ISP5	calculated	$CH_2CHCOO(CH_3)CH_2OH$
ISP6	calculated	$OOCH_2CHC(CH_3)CH_2OH$
MACP	calculated	$OHCC(CH_3)(O_2)CH_2OH + OHCC(CH_3)(OH)CH_2O_2$
MA2P	calculated	$CH_2C(CH_3)C(O)O_2$
MVKP	calculated	MVK peroxy
PNA	calculated	HO_2NO_2
MGLY	calculated	methyl glyoxal
KETP	calculated	acetone peroxy
ETEP	calculated	ethene hydroperoxy
OLTP	calculated	terminal olefin hydroperoxy
OLIP	calculated	internal olefin hydroperoxy
ETHP	calculated	CH_3CH_2OO
PROP	calculated	propylperoxy
TOLP	calculated	toluene peroxy
APIP	calculated	monoenyl terpene peroxy
LIMP	calculated	dienyl terpene peroxy
ISOP	input	isoprene
MACR	input	methacrolein
MVK	input	methyl vinyl ketone
MFUR	input	3-methyl furan
ETE	input	ethene
ETH	input	ethane
PRO	input	propane
OLI	input	internal alkene
OLT	input	terminal alkene
ALD	input	C2-C4 aldehydes
KET	input	acetone
PAN	input	peroxyacetyl nitrate
MPAN	input	$CH_2C(CH_3)C(O)O_2NO_2$

Table 3. Association and Equilibrium Reactions Used in the Model

Reaction	k_0^{300}	n	k_∞^{300}	m	Reference
		Association Reactions[a]			
$OH + NO \rightarrow HONO$	7.0E-31	2.6	3.6E-11	0.1	Dransfield
$HO_2 + NO_2 \rightarrow PNA$	1.8E-31	3.2	4.7E-12	1.4	DeMore
$OH + NO_2 \rightarrow HNO_3$	2.85E-30	2.67	3.13E-11		DeMore
$ACO3 + NO_2 \rightarrow PAN$	9.7E-29	5.6	9.3E-12	1.5	DeMore
$MA2P + NO_2 \rightarrow MPAN$	9.7E-29	5.6	9.3E-12	1.5	see below[a]
$OH + SO_2 \rightarrow HO_2 + SULF$	3.0E-31	3.3	1.5E-12		DeMore

Reaction	A	B	Reference
	Equilibrium Reactions[b]		
$HO_2 + NO_2 \leftrightarrow PNA$	2.1E-27	10900	DeMore
$ACO3 + NO_2 \leftrightarrow PAN$	1.3E-28	11200	DeMore
$MA2P + NO_2 \leftrightarrow MPAN$	1.3E-28	11200	see below[b]

[a] $k(\mathrm{cm}^3\ \mathrm{molecules}^{-1}\ \mathrm{s}^{-1}) = [k_0(T)[M]/(1 + k_0(T)[M]/k_\infty(T))]0.6^C$, where $C = 1/(1+[\log_{10}(k_0(T)[M]/k_\infty(T))]^2)$, $k_0(T) = k_0^{300}(T/300)^{-n}$, $k_\infty(Y) = k_\infty^{300}(T/300)^{-m}$, and $[M]$ is the concentration of air in molecules cm^3 [*DeMore et al.*, 1997]. The OH + NO_2 reaction takes a slightly different form: $k = k_0(T)[(\beta/(1 + \beta k_0(T)[M]/k_\infty(T))]F^{l}1/(1 + ((\log_{10}(\beta k_0(T)[M]/k_\infty(T)) - 0.12)/N)^2)]$, where $\beta = 0.933$, $F = \exp(-T/363)$, $N = 0.85-0.67\log_{10}(F)$ [*Dransfield et al.*, 1999]. Read 7.0E-31 as 7.0×10^{-31}.

[b] $K/(\mathrm{cm}^3\ \mathrm{molecules}^{-1}) = A\ \exp(B/T)[200 < T/K < 300]$. MPAN equilibrium kinetics are set equal to PAN.

glyoxals were calculated using the Madronich algorithm and scaled as a function of solar zenith angle to the Eppley-derived $j(NO_2)$. The uncertainties in the photolysis frequency calculations range from 25% to 50% (depending on the j value) at solar noon to a factor of 3 or more at high solar zenith angles (SZA).

OH has a midday lifetime of less than 100 ms at PROPHET, whereas for HO_2, the midday lifetime is on the order of 15-20 s. The steady-state assumption should therefore be valid during the day; it may fail at night, however, so the validity of the model runs is restricted to conditions when the solar zenith angle was less than 60° (about 0800 to 1600 solar time). This restriction also reduces the error in j values inherent at large SZA. The production terms for species X are set equal to the loss terms, and the set of simultaneous equations solved

$$P_X - L_X[X] = 0. \quad (1)$$

The model is written in MATLAB (Mathworks, Natick, Massachussetts), and uses a nonlinear equation solver. The model calculates 30 min average concentrations of OH and HO_2, as well as those of PNA, methyl glyoxal, and the peroxy radicals of isoprene, methacrolein, MVK, acetone, methane, acetyl, toluene, ethane, ethene, propane, terminal alkenes such as propene and 1-butene, internal alkenes such as *cis*- and *trans*-butene and 2-pentenes, and terpenes. These latter were lumped as either monoenyl (APIP in the model) or dienyl (LIMP) terpene peroxy radicals. The model takes as input 30 min average values of ozone, NO, NO_2, CO, water vapor, isoprene, methacrolein, MVK, 3-methyl furan, formaldehyde, acetaldehyde, acetone, the measured terpenes, including α-pinene and β-pinene, toluene, peroxyacetyl nitrate (PAN), peroxymethacryloyl nitrate (MPAN), and SO_2, and the calculated photolysis frequencies and aerosol surface area. Where the Purdue GC/MS data and the NCAR GC/MS data overlapped, the Purdue data were used for isoprene and 3-methyl furan and the NCAR data for acetone, acetaldehyde, methacrolein, and MVK. Data points below the limit of detection were set to one-half the value of the limit of detection. All data were merged to a common 30 min time stamp for modeling use. Levels of ethane, ethene, propane, and internal and terminal olefins (OLI and OLT in the model, respectively) are set equal to mean concentrations of those species as measured by whole-air sampling as performed by Ohio University at 35 time points during the intensive. Methane is assumed to be a constant 1710 parts-per-billion-by-volume (ppbv), H_2O_2 a constant 2 ppbv, and CH_3OOH 500 pptv. Nitric acid was not measured (although 24 hour averaged acidic gas data are available) but set equal to NO_y - $1.15\times(NO + NO_2 + PANs)$.

Table 4. Second-Order Reactions Used in the Model

Reaction	k(molecules/cm^3)	$-E/R$	Reference
$O^1D + H_2O \rightarrow 2$ OH	2.2E-10		DeMore
$O^1D + N_2 \rightarrow O^3P$	1.8E-11	110	DeMore
$O^1D + O_2 \rightarrow O^3P$	3.2E-11	70	DeMore
O_3 + ISO → 0.27 OH + 0.09 MO2 + 0.11 HO_2 + products	7.86E-15	-1913	Atkinson
O_3 + MVK → 0.46 OH + 0.24 MO2 + 0.76 MGLY + 0.7 HCHO + products	4.0E-15	-2000	Atkinson
O_3 + MACR → 0.46 OH + 0.76 MGLY + 0.7 HCHO + products	4.4E-15	-2500	Atkinson
O_3 + APIN → 0.85 OH + products	1.01E-15	-732	Atkinson
O_3 + BPIN → 0.35 OH + products	1.5E-17		Atkinson
O_3 + myrcene → 1.15 OH + products	4.7E-16		Atkinson
O_3 + camphene → 0.18 OH + products	9.0E-19		Atkinson
O_3 + Δ^3-carene → 1.06 OH + products	3.7E-17		Atkinson
O_3 + limonene → 0.86 OH + products	2.0E-16		Atkinson
O_3 + γ-terpinene → products	1.4E-16		Atkinson
O_3 + α-humulene → 0.22 OH + products	1.17E-14		Atkinson
O_3 + ETE → 0.12 OH + 0.26 HO_2 + HCHO + products	9.14E-15	-2580	Stockwell
O_3 + OLT → 0.40 OH + 0.25 HO_2 + 0.19 MO2 + 0.64 HCHO + 0.44 ALD + 0.03 KET + 0.03 KETP + 0.10 ETHP + products	4.33E-15	-1800	Stockwell
OH + HO_2 → H_2O + O_2	4.8E-11	250	DeMore
OH + O_3 → HO_2 + O_2	1.6E-12	-940	DeMore
OH + HOOH → H_2O + HO_2	2.9E-12	-160	DeMore
OH + CH_3OOH → 0.5 OH + 0.5 MO2 + 0.5 HCHO	1.0E-11		Stockwell
OH + HO_2NO_2 → H_2O + NO_2 + O_2	1.3E-12	380	DeMore
OH + CH_3COCH_3 → KETP	2.2E-12	-685	DeMore
OH + CH_3CO → ACO3 + H_2O	5.6E-12	270	DeMore
OH + MGLY → ACO3 + CO + H_2O	1.72E-11		Stockwell
OH + ISO → 0.1ISP1 + 0.19 ISP2 + 0.11 ISP3 + 0.17 ISP4 + 0.27 ISP5 + 0.16 ISP6	2.54E-11	410	Atkinson
OH + MACR → 0.5 MACP + 0.5 MA2P	1.86E-11	175	Zimmerman
OH + MVK → MVKP	4.13E-12	452	Zimmerman
OH + MFUR → MFUP	6.0E-11		Zimmerman
OH + α-pinene → APIP	1.21E-11	444	Atkinson
OH + β-pinene → APIP	2.38E-11	357	Atkinson
OH + myrcene → LIMP	9.4E-11		Atkinson
OH + camphene → APIP	5.3E-11		Atkinson
OH + Δ^3-carene → APIP	8.8E-11		Atkinson
OH + limonene → LIMP	1.71E-10		Atkinson
OH + α-phellandrene → LIMP	3.13E-10		Atkinson
OH + γ-terpinene → LIMP	1.77E-10		Atkinson
OH + α-humulene → products	2.93E-10		Atkinson
OH + CH_4 → MO2	2.45E-12	-1775	DeMore
OH + C_2H_6 → ETHP	8.7E-12	-1070	DeMore
OH + C_3H_8 → PROP	1.0E-11	-660	DeMore
OH + ETE → ETEP	1.96E-12	438	Stockwell
OH + OLT → OLTP	5.72E-12	500	Stockwell
OH + OLI → OLIP	1.33E-11	500	Stockwell
OH + toluene → 0.10 HO_2 + 0.90 TOLP + products	1.81E-12	355	Stockwell
OH + MPAN → 0.40 HO_2 + products	3.25E-13	500	Stockwell
HO_2 + O_3 → OH + 2 O_2	1.1E-14	-500	DeMore
HO_2 + MO2 → CH_3OOH	3.8E-13	800	DeMore
HO_2 + ACO3 → products	4.5E-13	1000	DeMore
HO_2 + NO → OH + NO_2	3.5E-12	250	DeMore
HO_2 + ISP → ISOOH	1.63E-11		Jenkin
HO_2 + MACP, MA2P, MVKP, MFUP → ROOH	1.28E-13	1300	Zimmerman
HO_2 + APIP, LIMP → ROOH	1.50E-11		Stockwell
HO_2 + TOLP → ROOH	4.2E-14	980	Stockwell
HO_2 + KETP → ROOH	1.15E-13	1300	Stockwell

Table 4. (continued)

Reaction	k(molecules/cm^3)	$-E/R$	Reference
HO_2 + ETEP → ROOH	1.9E-13	1300	Stockwell
HO_2 + OLTP, OLIP → ROOH	1.66E-13	1300	Stockwell
HO_2 + ETHP → ROOH	7.5E-13	700	DeMore
HO_2 + PROP →	6.0E-12		Makar
MO2 + NO → HO_2 + HCHO	3.0E-12	280	DeMore
MO2 + MO2 → 2 HO_2 + 2 HCHO + O_2	2.5E-13	190	DeMore
MO2 + ACO_3 → HCHO + HO_2 + MO2	3.21E-11	-440	Stockwell
MO2 + ACO_3 → HCHO + products	2.68E-16	2510	Stockwell
MO2 + ISP → HO_2 + products	2.0E-12		Jenkin
MO2 + APIP → 2 HO_2 + HCHO + products	3.56E-14	708	Stockwell
MO2 + LIMP → 2 HO_2 + 1.4 HCHO + 0.6 MACR + 0.6 OLI	3.56E-14	708	Stockwell
MO2 + ETEP → 1.55 HCHO + HO_2 + 0.35 ALD	1.71E-13	708	Stockwell
MO2 + TOLP → HCHO + HO_2 + 0.35 MGLY + products	3.56E-14	708	Stockwell
MO2 + KETP → 0.88 HO_2 + 0.75 HCHO + 0.40 MGLY + 0.12 ACO_3 + products	6.91E-13	508	Stockwell
MO2 + OLTP → HO_2 + 1.25 HCHO + 0.669 ALD + 0.081 ALD	1.46E-13	708	Stockwell
MO2 + OLIP → HO_2 + 0.755 HCHO + 0.669 ALD + 0.81 KET	9.18E-14	708	Stockwell
MO2 + ETHP → HO_2 + 0.75 HCHO + 0.75 ALD	1.18E-13	158	Stockwell
MO2 + PROP → HO_2 + 0.75 HCHO + 0.25 MO2	9.8E-14	-100	Makar
ACO3 + ACO3 → 2 MO2	2.8E-12	530	Stockwell
ACO3 + APIP → HO_2 + MO2 + ALD + KET	7.4E-13	765	Stockwell
ACO3 + LIMP → HO_2 + MO2 + 0.6 MACR + 0.4 OLI + 0.4 HCHO	7.4E-13	765	Stockwell
ACO3 + TOLP → HO_2 + MO2 + 0.35 MGLY + products	7.4E-13	765	Stockwell
ACO3 + KETP → 0.38 HO_2 + 0.5 MO2 + 0.54 MGLY + 0.12 ACO3 + products	7.51E-13	765	Stockwell
ACO3 + ETEP → 0.5 HO_2 + 0.5 MO2 + 0.8 HCHO + 0.6 ALD + products	9.48E-13	765	Stockwell
ACO3 + OLTP → 0.501 HO_2 + 0.501 MO2 + 0.501 HCHO + 0.849 ALD + 0.151 KET + products	8.11E-13	765	Stockwell
ACO3 + OLIP → 0.51 HO_2 + 0.51 MO2 + 0.941 ALD + 0.569 KET + products	5.09E-13	765	Stockwell
ISP1, ISP2, ISP3, ISP4, ISP5, ISP6 + NO → 0.9 HO_2 + 0.1 $RONO_2$ + products	3.8E-12		Jenkin
ISP1, ISP2, ISP3, ISP4, ISP5, ISP6 + HO_2 → ROOH	1.63E-11		Jenkin
ISP1, ISP2, ISP3, ISP4, ISP5, ISP6 + MO2 → + HO_2 + products	2.0E-12		Jenkin
ISP1, ISP3, ISP4, ISP6 + MACP → 1.2 HO_2 + 0.6 MGLY + products	1.5E-13		Zimmerman
ISP2 + MACP → 1.2 HO_2 + 0.6 MGLY + 1.2 HCHO + 0.6 MACR + 0.3 OLI + products	5.0E-15		Zimmerman
ISP5 + MACP → 1.2 HO_2 + 0.6 MGLY + 1.2 HCHO + 0.6 MVK + 0.3 OLI + products	8.0E-16		Zimmerman
ISP1, ISP3, ISP4, ISP6 + MA2P → 0.8 HO_2 + 0.8 ACO3 + products	1.0E-12		Zimmerman
ISP2 + MA2P → 0.8 HO_2 + 0.8 ACO3 + 1.6 HCHO + 0.2 OLI + products	6.0E-14		Zimmerman
ISP5 + MA2P → HO_2 + ACO3 + 2 HCHO + MVK	1.0E-14		Zimmerman
ISP1, ISP3, ISP4, ISP6 + MVKP → 1.2 HO_2 + 0.6 MGLY + products	1.5E-13		Zimmerman
ISP2 + MVKP → 1.2 HO_2 + 0.6 MGLY + 0.6 MACR + 1.2 HCHO + 0.3 OLT + products	5.0E-15		Zimmerman

Table 4. (continued)

Reaction	k(molecules/cm^3)	-E/R	Reference
ISP5 + MVKP → 1.2 HO_2 + 0.6 MGLY + 0.6 MVK + 1.2 HCHO + 0.3 OLT + products	8.0E-16		Zimmerman
ISP1 + ISP1 → 1.2 HO_2 + products	4.8E-12		Jenkin
ISP1 + ISP2 → 1.4 HO_2 + products	5.17E-12		Jenkin
ISP1 + ISP3 → 1.21 HO_2 + products	3.65E-12		Jenkin
ISP1 + ISP4 → 1.2 HO_2 + products	4.8E-12		Jenkin
ISP1 + ISP5 → 1.6 HO_2 + products	2.57E-12		Jenkin
ISP1 + ISP6 → 1.21 HO_2 + products	4.74E-12		Jenkin
ISP2 + ISP2 → 1.6 HO_2 + products	5.74E-12		Jenkin
ISP2 + ISP3 → 1.41 HO_2 + products	3.94E-12		Jenkin
ISP2 + ISP4 → 1.4 HO_2 + products	5.17E-12		Jenkin
ISP2 + ISP5 → 1.8 HO_2 + products	3.08E-12		Jenkin
ISP2 + ISP6 → 1.41 HO_2 + products	3.94E-12		Jenkin
ISP3 + ISP3 → 1.22 HO_2 + products	2.77E-12		Jenkin
ISP3 + ISP4 → 1.21 HO_2 + products	3.65E-12		Jenkin
ISP3 + ISP5 → 1.61 HO_2 + products	2.49E-12		Jenkin
ISP3 + ISP6 → 1.22 HO_2 + products	3.29E-12		Jenkin
ISP4 + ISP4 → 1.2 HO_2 + products	4.8E-12		Jenkin
ISP4 + ISP5 → 1.6 HO_2 + products	2.57E-12		Jenkin
ISP4 + ISP6 → 1.21 HO_2 + products	4.74E-12		Jenkin
ISP5 + ISP5 → 2 HO_2 + products	6.92E-14		Jenkin
ISP5 + ISP6 → 1.61 HO_2 + products	2.49E-12		Jenkin
ISP6 + ISP6 → 1.22 HO_2 + products	3.9E-12		Jenkin
MACP + NO → HO_2 + NO_2 + 0.2 MGLY 0.8 CO + 0.2 HCHO + products	4.2E-12	180	Zimmerman
MA2P + NO → ACO3 + HCHO + NO_2 + CO_2	2.40E-11		Zimmerman
MA2P + ACO3 → MO2 + ACO3 + HCHO	1.19E-12	220	Zimmerman
MA2P + MA2P → 2 ACO3 + 2 HCHO	1.19E-12	220	Zimmerman
MVKP + NO → 0.3 HO_2 + 0.3 MGLY + 0.1 ACO3 + 0.3 HCHO + NO_2 + products	4.2E-12	180	Zimmerman
MFUP + NO → HO_2 + 0.5 MACR + 0.5 MVK + NO_2	4.2E-12	180	Zimmerman
APIP + NO → 0.80 HO_2 + 0.80 ALD + 0.80 KET 0.80 NO_2 + 0.20 $RONO_2$	4.0E-12		Stockwell
LIMP + NO → 0.65 HO_2 + 0.4 MACR + 0.25 HCHO + 0.65 NO_2 + 0.25 OLI + 0.35 $RONO_2$	4.0E-12		Stockwell
KETP + NO → HO_2 + MGLY + NO_2	4.2E-12	180	Zimmerman
ETEP + NO → HO_2 + 1.6 HCHO + 0.2 ALD + NO_2	9.0E-12		Stockwell
OLTP + NO → HO_2 + HCHO + NO_2 + 0.94 ALD + 0.06 KET	4.0E-12		Stockwell
OLIP + NO → HO_2 + 1.71 ALD + 0.29 KET + NO_2	4.0E-12		Stockwell
ETHP + NO → 0.99 HO_2 + 0.99 ALD +0.99 NO_2 + $RONO_2$	2.6E-12	365	Stockwell
PROP + NO → 0.96 HO_2 + 0.96 NO_2 + ALD + 0.04 $RONO_2$	5E-12		Makar
TOLP + NO → HO_2 + NO_2 + 0.17 MGLY + products	4.0E-12		Stockwell
OH + CO → H + CO_2	1.5E-13×(1+5.9E-4(P))		DeMore
OH + HCHO → HO_2 + H_2O + CO	1.20E-14 ×T × exp(287/T)		Atkinson
HO_2 + HO_2 → H_2O_2 + O_2	(2.3E-13 exp(600/T) +1.7E-33[M] exp(1000/T)) ×(1+1.4E-21[H_2O][M] exp(2200./T))		DeMore

P is ambient pressure in mbar, T is ambient temperature in Kelvins, and [M] is the concentration of air in molecules/cm^3.

Table 5. Median and Maximum Values of Chemical Species and Photolysis Frequencies Used As Input to the Model

Species	Median	Maximum	Comment
NO	65.8 pptv	598.8 pptv	measured
NO_2	591.9 pptv	3045 pptv	measured
O_3	49.2 ppbv	88.3 ppbv	measured
CO	260.3 ppbv	489 ppbv	measured
HCHO	3.8 ppbv	10.6 ppbv	measured
Acetaldehyde	2.7 ppbv	10.6 ppbv	measured
Isoprene	2.5 ppbv	6.9 ppbv	measured
Methacrolein	227 pptv	241 pptv	measured
MVK	114 pptv	733 pptv	measured
3-methylfuran	21 pptv	86 pptv	measured
α-pinene	15.6 pptv	87.3 pptv	measured
β-pinene	11.9 pptv	225 pptv	measured
Camphene	1.4 pptv	9.4 pptv	measured
Myrcene	5.7 pptv	28 pptv	measured
Δ^3-carene	4.7 pptv	87 pptv	measured
Toluene	59 pptv	217 pptv	measured
$j(O^1D)$		2.4×10^{-5} sec^{-1}	calculated
$j(NO_2)$		8.7×10^{-3} sec^{-1}	calculated
$j(HCHO \rightarrow HO_2)$		2.7×10^{-5} sec^{-1}	calculated
$j(HCHO \rightarrow H_2)$		4.0×10^{-5} sec^{-1}	calculated
j(acetone)		9.0×10^{-7} sec^{-1}	calculated
j(aldehyde) $\rightarrow HO_2 + ...$		4.5×10^{-6} sec^{-1}	calculated
j(methyl glyoxal)		1.7×10^{-4} sec^{-1}	calculated
$j(H_2O_2)$		6.7×10^{-6} sec^{-1}	calculated
$j(CH_3OOH)$		6.6×10^{-6} sec^{-1}	calculated
$j(NO_2)$		8.7×10^{-3} sec^{-1}	calculated
j(PNA)		5.6×10^{-6} sec^{-1}	calculated
HNO_3	0.29 ppbv	5.9 ppbv	see text
H_2O_2	2 ppbv		see text
CH_3OOH	0.5 ppbv		see text
Methane	1710 ppbv		see text
Ethane	1 ppbv		see text
Propane	0.36 ppbv		see text
Ethene	0.18 ppvb		see text
Terminal olefins	0.42 ppbv		see text
Internal olefins	0.17 ppbv		see text

The assumption of constant concentrations for peroxides, alkanes, and some alkenes, and the treatment of nitric acid are clearly unrealistic; however, the values should be representative of the concentrations of those species. For details about the surface area calculations, see *Faloona et al.*, [this issue]; an uptake coefficient of $\gamma = 0.05$ was used in the model, and all of the aerosol was assumed to be sulfate. A complete listing of the species calculated by the model is provided in Table 2. Certain of the species, particularly the terpenes and toluene, were measured only during a span from August 5 to 15. The model treatment therefore only includes this time span, not the entire intensive. The uncertainty in the model is estimated to be typically a factor of about 2.6 for OH and a factor of about 2.1 for HO_2 and is driven primarily by the uncertainties in the j value calculations and in the rate constants for OH + isoprene and RO_2 + NO. It should be noted, however, that the rate constants for many if not most of the reactions important in this environment are not known and are estimated by similarity theory, and that the mechanisms, including branching ratios and product yields, are typically established for different conditions (e.g., much higher levels of NO.)

Table 5 presents median and maximum measured values for many of the species and photolysis frequencies important to HO_x. Because isoprene is thought to be a key player in this environment, isoprene oxidation is treated in some detail. Isoprene is a diene, and the reaction with OH goes by addition. OH can add to form six different hydroperoxy radical isomers [*Paulson et al.*, 1992], each of which is calculated here, using kinetic data from *Jenkin et al.*, [1998]. These isoprene peroxy radicals (ISP1-ISP6 in Table 5; total isoprene peroxy radicals is denoted by ISP) may react with NO, each other, or other RO_2 (RO_2 in this paper includes the peroxyacetyl radical, denoted by ACO3 in Table 5, but not HO_2) to form HO_2, formaldehyde, and larger decom-

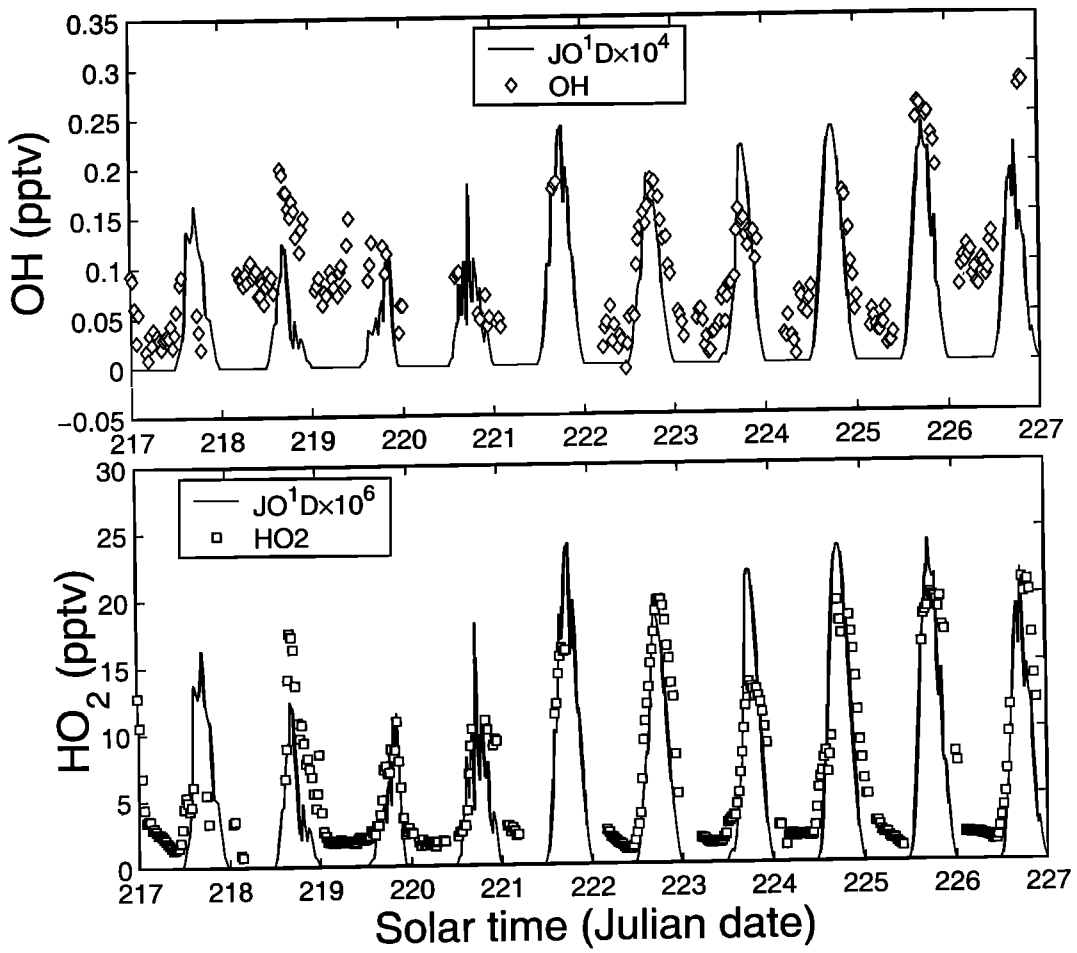

Figure 3. Time series of the HO_x data collected during the PROPHET'98 campaign. The time base is solar time in Julian date. The solid line is the calculated $j(O^1D)$, scaled by the factor shown. The symbols denote the data points.

position products, including MVK and methacrolein. They may also react with HO_2, forming organic hydroperoxides. This is true for all RO_2; however, because of the high reactivity of isoprene to OH and the high levels of isoprene measured at PROPHET, the isoprene peroxy radicals form the majority of RO_2 at PROPHET 1998.

4. Results

Figure 3 shows a time series of the OH and HO_2 data measured during PROPHET 1998. Midday OH mixing ratios ranged from about 0.10 to 0.20 pptv, whereas HO_2 ranged from about 10 to nearly 25 pptv. Most of the variation is driven by insolation. Neither OH nor HO_2 go to zero at night: OH stayed well above the detection limit throughout the night for nearly all nights, and considerable structure is noticeable in the HO_2 nighttime profile. These remarkable findings are discussed in detail by *Faloona et al.*, [this issue]. The solid line is $j(O^1D)$, scaled by the factor shown. The model runs extend from Julian dates 217 to 225.

Scatter plots of model against observations for OH and HO_2 are shown in Figure 4. The dashed lines have slopes equal to the mean deviation between the observed data points and the model predictions; the crosshair denotes the typical model and measurement uncertainties. Agreement between model and observation for OH is quite poor; the model consistently and considerably underpredicts the measured OH. OH observations are in the mean 2.66 times higher than the model prediction. The model, moreover, is unable to predict the variability in detail of the measured OH. For HO_2, however, the agreement between model and observation is very good, perhaps fortuitously good, given the uncertainty in the model. The model overpredicts the observations in the mean by less than 15%, well within the uncertainty of both model and measurement, and measured variability is captured reasonably well.

More detail can be seen in the diurnal profiles of model and observation, as shown in Figure 5. Here, the symbols denote median values of the data at each 30 min time point, and the solid line denotes median model values at each time point (see below for dot-

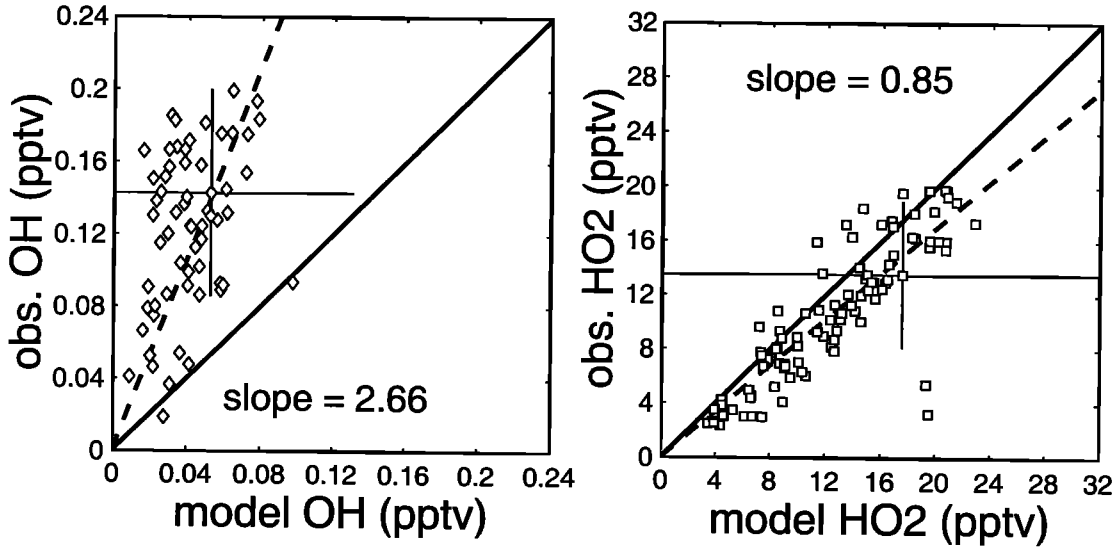

Figure 4. Scatterplots of the steady-state model versus the observed data. The solid line is the one-to-one line; the dashed line shows the mean deviation between the model and the measurements. Both the model and the data were restricted to solar zenith angles of less than 60°, and within the time span between August 5 and 13. The crosshairs denote the measurement and model uncertainties. Note that the dashed line is a comparison between the model and the observation: it is not a fit of the model to the data.

ted and dashed lines). The model underpredicts OH at all times; however, the lack of agreement is smallest in the morning hours between 0800 and 1000 solar time, after which agreement becomes markedly worse. The median diurnal profile of the HO_2 model is in excellent agreement with the observation at all times. The model underpredicts slightly after 1415 solar time. The reason for the diurnal asymmetry in the HO_x observed to model ratio appears to lie in the behavior of NO. NO shows a persistent morning peak, rising to several hundred pptv in the morning, then falling off rapidly to well below 100 pptv in the afternoon (see Figure 6a.) In addition, isoprene peaks in the early afternoon (Figure 6b): hence the OH source from $HO_2 + NO \rightarrow OH + NO_2$ is greatest in the morning, whereas the OH sink to isoprene is greatest in the afternoon. Figures 6d and 6e show the median diurnal profiles of ozone and $j(O^1D)$, respectively. Figure 6c shows the observed to model

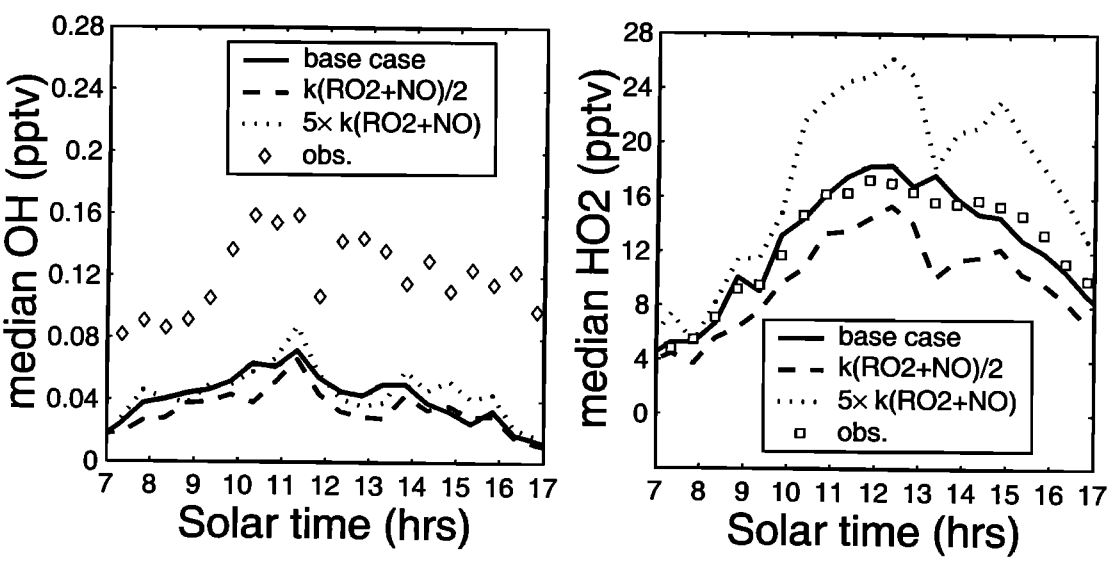

Figure 5. Diurnal median values for model (solid line) and observation (symbols). The time base is eastern daylight time (local time). The model runs should only be considered between approximately 0800 and 1600 EDT (SZA< 60°). The dashed line is the model run with the rate constants for higher-order $RO_2 + NO$ set at half the literature value; the dotted line is the model run with k_{RO2+NO} set at 5 times the literature value. The measured OH and HO_2 were used as a common data basis in the calculation of the median values.

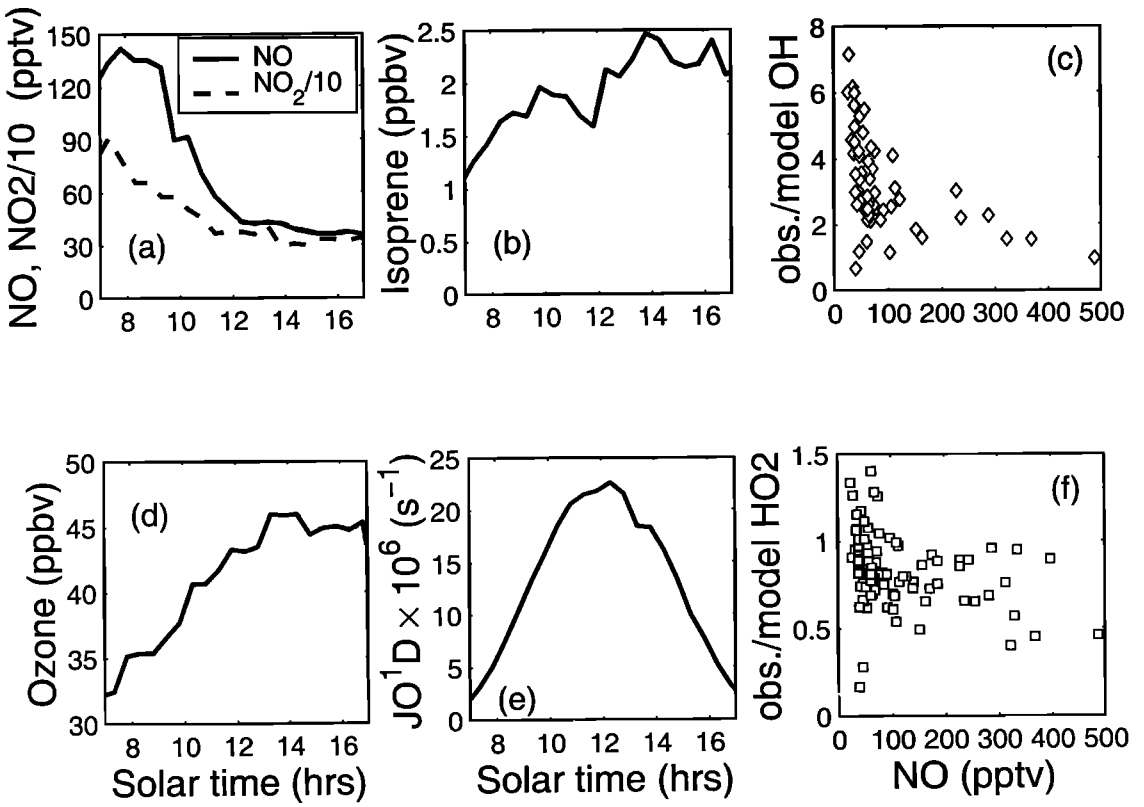

Figure 6. (a) Median daytime profiles of NO and NO_2. There is a persistent morning peak in NO reaching to several hundred parts-per-trillion-by-volume which correlates well with deviations between model and observed data. (b) Daytime median profile of isoprene. (d, e) Daytime median profiles of ozone and $j(O^1D)$. (c, f) Observed-to-model ratios of OH and HO_2 with respect to NO.

ratio of OH as a function of NO. At NO levels below 100 pptv, the agreement between model and measurement is extremely poor, with the model at times underpredicting the observation by a factor of 6 or more; it improves with increasing NO. The model HO_2 (Figure 6f) matches the data best at low NO, however. A similar trend exhibits itself in the HO_2/OH ratio (Figure 7) (the dashed line is the mean value of the ratio of the model to the observed HO_2/OH ratios.) Observed values of this ratio typically range from 80-120; the model expects nearly 4 times the observed. The deviation between the observed and the model ratios is greatest at very low NO (< 50 pptv); however, the deviation (expressed as the ratio of observed to model HO_2/OH ratios) does not converge to unity at high levels of NO.

Further insight into the HO_x system can be gleaned from the speciation of the HO_x budgets as shown in Figure 8. Figure 8 shows daytime median values for most of the sources and sinks of HO_x as calculated by the model, including all of the important ones. As expected, the strongest source of HO_x comes from the photolysis of ozone followed by reaction with water vapor, $O^1D + H_2O \rightarrow 2\ OH$, with a median value of 4×10^6 molecules/(cm^3• s). This is followed by the photolysis of formaldehyde (about 3.1×10^6 molecules/(cm^3• s)) and the ozonolysis of olefins, including isoprene (1×10^6 molecules/(cm^3• s)). The dominant sink of HO_x in this environment is the reaction of HO_2 with RO_2, which consumes about 2.8×10^6 molecules/(cm^3• s).

The observation of elevated nighttime OH and the poor performance of the model indicate that there may be an OH source not included in the model. In the work of *Faloona et al.*, [this issue] we speculate that this nonphotolytic source is the ozonolysis of reactive terpenes not measured during the PROPHET intensive. The actual terpene is not known; however, the nighttime behavior seems to correlate well to the monoterpene Δ^3-carene. For modeling purposes, an unspecified terpene with the temporal profile of Δ^3-carene, the reactivity to ozone of the sesquiterpene α-humulene, and unity OH yield was used. The concentration of the reactive terpene was adjusted to match nighttime OH levels, or a median daytime value of about 18 pptv. However, while such a concentration is similar to that of the pinenes at PROPHET, the source strength of the hypothetical terpene must be $\sim$ 20 times greater than the pinene source strengths, because the reactivity of the hypothetical terpene is much greater than that of the pinenes.

Inclusion of this additional source improves the model prediction with respect to OH; the data are still greater

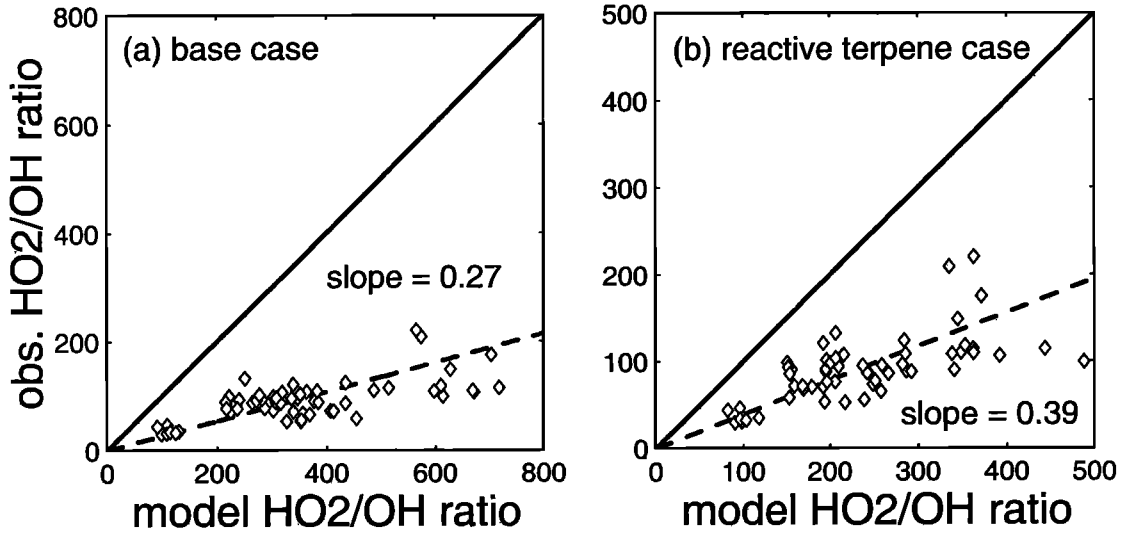

Figure 7. (a) Scatterplot of the observed and model HO_2/OH ratios. The dashed line is the mean deviation between the observed and the modeled ratios. (b) Same plot for the reactive terpene case.

than the model, however, by a factor of 1.5 (Figure 9.) The agreement between model and measured HO_2 becomes slightly worse but still acceptable, with the model overpredicting the observations by ~30%. Median diurnal profiles of model HO_x with the additional terpene source are shown in Figure 10, along with the diurnal profiles of the observed data. As in the model base case, the model OH agrees best with the observations in the morning, when NO is high, and less well later in the day, when NO is low. Model HO_2 is higher than measured at all times, with the overprediction somewhat worse in the morning and improving in the afternoon. The HO_2/OH ratio is improved with the inclusion of the reactive terpene term (Figure 7b), but the model ratio is still ~ 2.5 times the observed ratio. The agreement between the observed and the model ratios does not depend on NO.

A detailed budget for the reactive terpene case is shown in Figure 11. The primary source of OH is now the ozonolysis of reactive terpenes, which has a source strength of close to twice the O^1D+ H_2O source. This source alone is on the order of the cycling from HO_2 by NO and O_3. HO_2 itself increases, both directly from OH + CO, OH + O_3, and OH + HCHO reactions, and from RO_2 + NO. RO_2 is now, on average, as much a sink of HO_2 through the formation of hydroperoxides, RO_2 + HO_2 → ROOH + O_2, as it is a source. Median RO_2 increases from a maximum of 32 pptv at noon in the

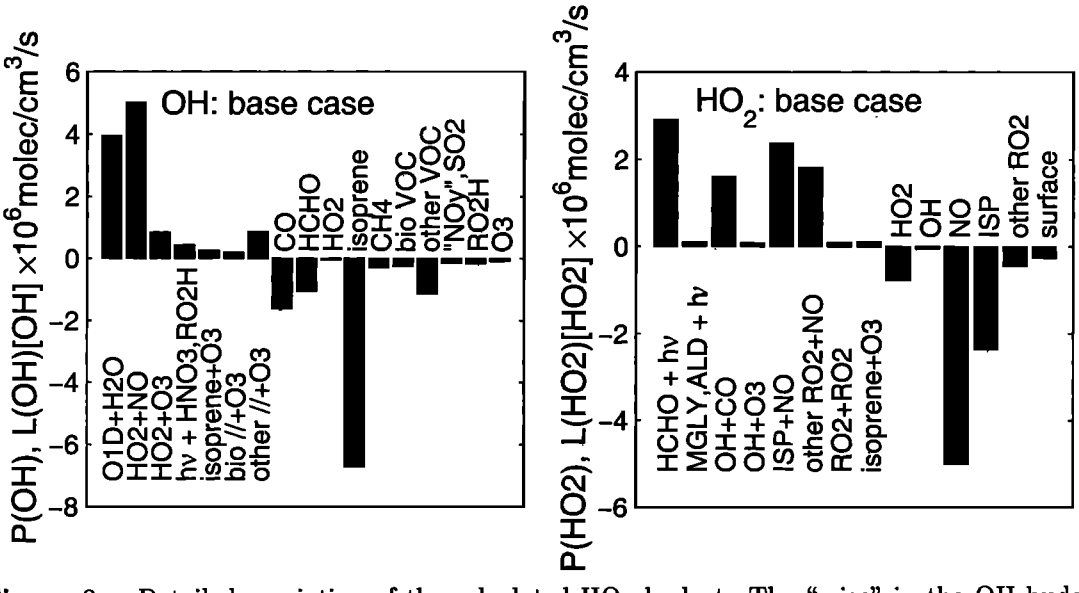

Figure 8. Detailed speciation of the calculated HO_x budget. The "misc" in the OH budget refers to NO_2, HNO_3, SO_2, and PNA. "RO_2 + RO_2" in the HO_2 source term refers to non-ISP RO_2. The primary source of HO_x during PROPHET 1998 was the reaction of O^1D+ H_2O, followed by the photolysis of HCHO and the ozonolysis of olefins ("//"). The primary sink of HO_x was reaction with RO_2, followed by the self-reaction of HO_2.

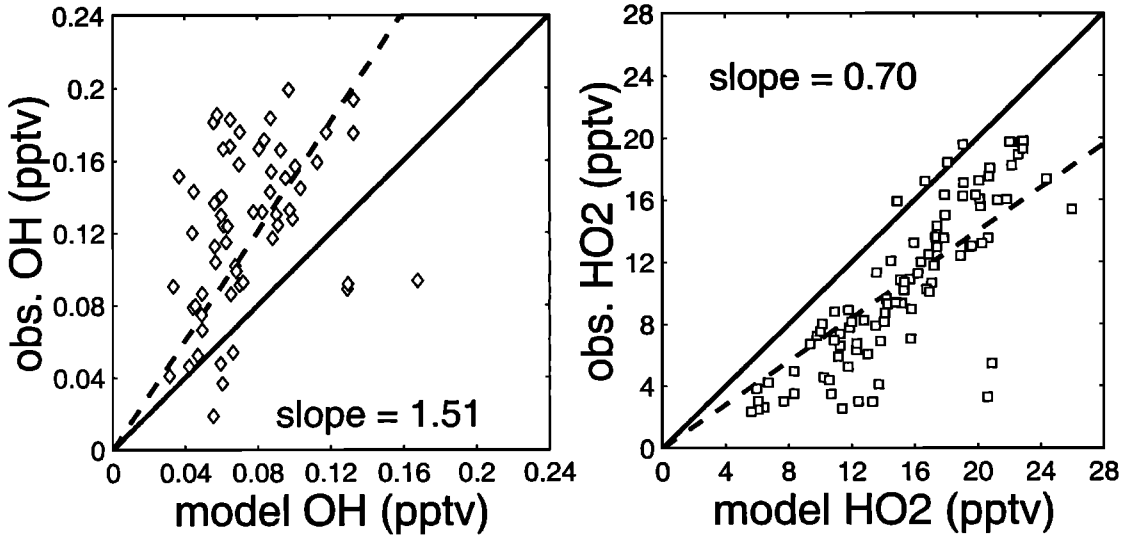

Figure 9. Scatterplots of the observed data and the model predictions when an additional OH source sufficient to match nighttime observations is included in the model.

base model case to 46 pptv at about 1400 (Figure 12). The fraction of RO_2 made up of isoprene peroxy radicals also increases, from two thirds to over 75%, in the median sense. Both the base case RO_2 and the reactive terpene case RO_2 are within rough agreement with total RO_2 measurements taken by the chemical amplifier technique during the PROPHET summer 1997 intensive (C. Mihele, private communication, 2000). (This assumes that HO_2 in PROPHET 1997 was similar to HO_2 in PROPHET 1998, since the measurement was of total $RO_x = RO_2 + HO_2$.) Unfortunately, RO_2 was not measured in the PROPHET 1998 campaign, so no direct comparisons can be made.

Total RO_2 is often estimated using the deviations from simple photostationary steady state (PSS), which uses the NO_2/NO ratio to calculate RO_x:

$$[RO_2] \approx \frac{1}{k_1} \times \left[\frac{j(NO_2)[NO_2]}{[NO]} - k_2[HO_2] - k_3[O_3]\right], \quad (2)$$

where $k_1 = k_{RO_2+NO}$, $k_2 = k_{HO_2+NO}$, and $k_3 = k_{O_3+NO}$. This approach is sensitive to RO_2 speciation and is at best appropriate near solar noon. The PSS RO_2 (not including HO_2, which is a measured constraint, as are ozone, NO, and NO_2) is shown in Figure 13. The dashed line is the estimate assuming that all of the RO_2 + NO rate constants are that of MO2 + NO, whereas the solid line assumes that one third of the RO_2 + NO rate constants are that of MO2 + NO and that two thirds are that of ISP + NO (the branching is chosen roughly to match the results of the full point model.) Even the more conservative of the two PSS estimates is much

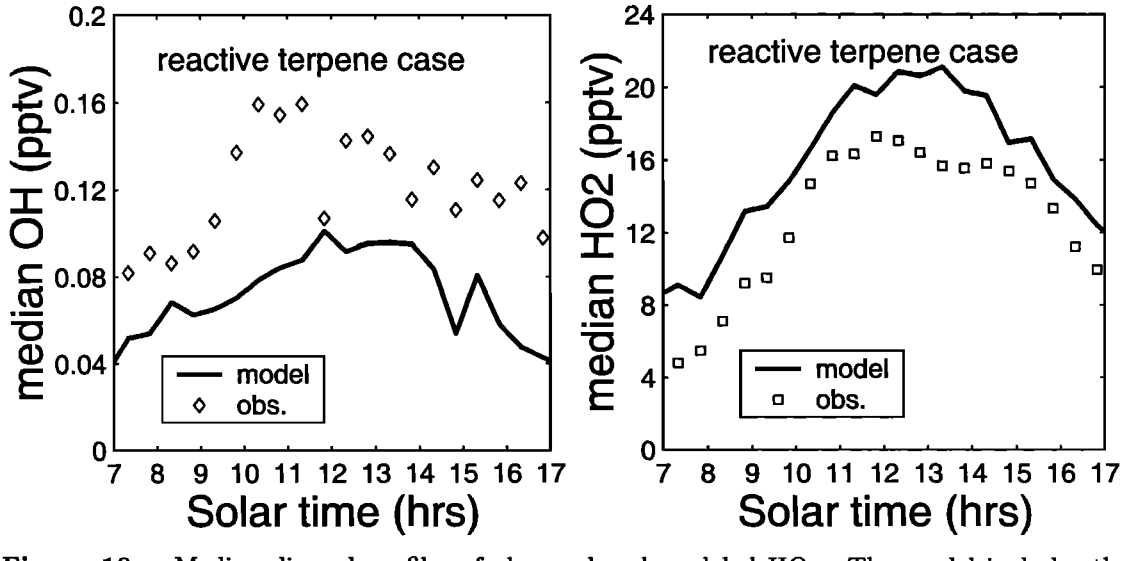

Figure 10. Median diurnal profiles of observed and modeled HO_x. The model includes the additional OH source from terpene ozonolysis. The measured OH and HO_2 were used as a common data basis in the calculation of the median values.

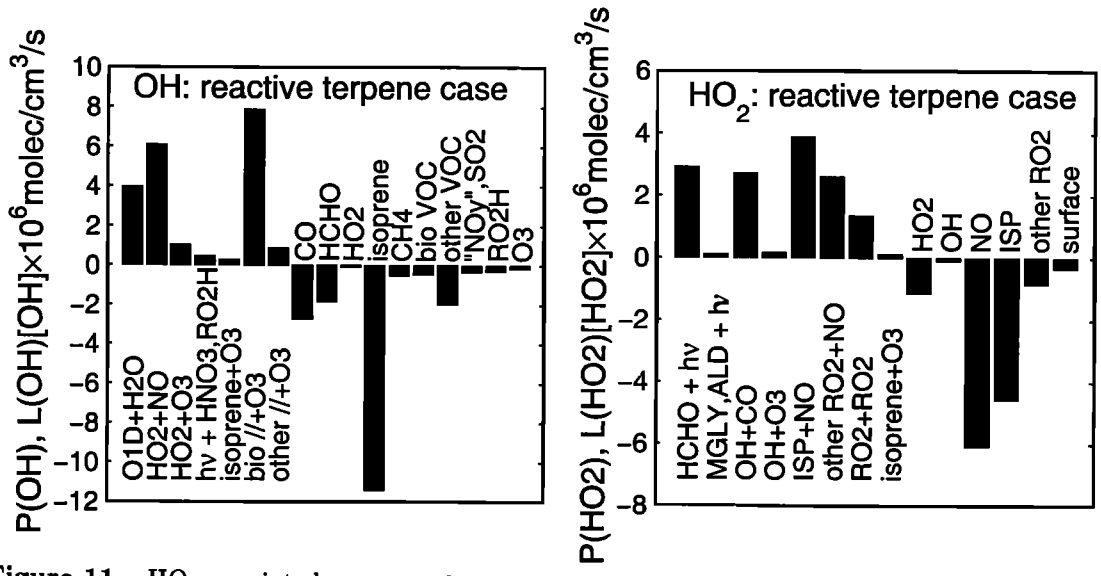

Figure 11. HO_x-speciated source and sink strengths for the reactive terpene model case. The ozonolysis of reactive terpenes is now the primary HO_x source, with a source strength nearly twice that of $O^1D + H_2O$.

higher than either case of the point model and the measurements from PROPHET 1997. The behavior of the PSS RO_2 with respect to RO_2 as calculated in the point model is similar to that found by *Cantrell et al.*, [1997] during TOHPE. It is probable that the PSS calculations for RO_2 are not appropriate for this environment. In any case, the large uncertainties in the concentrations and speciation of RO_2 as well as in the mechanisms of RO_2 reactions point to open questions concerning the nature and fate of RO_2 in this environment.

5. Discussion

The present constrained model efforts to understand OH and HO_2 in a high isoprene, low NO environment do poorly in simulating observed values of OH but reasonably well in simulating the observed HO_2 concentrations. There are two major shortcomings: the predicted OH is much lower than the measured OH, and the predicted HO_2/OH ratio is much higher than the measured ratio. Several possibilities exist to explain the discrepancies. (1) There may be a problem with the OH (but not HO_2) measurement. (2) There may be a problem with one of the supporting measurements which provide input to the constrained model. (3) Species important to HO_x were present at the PROPHET intensive but not measured. (4) There may be a problem with the model. We examine each possibility in order.

We cannot exclude the possibility of a problem with the OH measurement. The PROPHET summer 1998

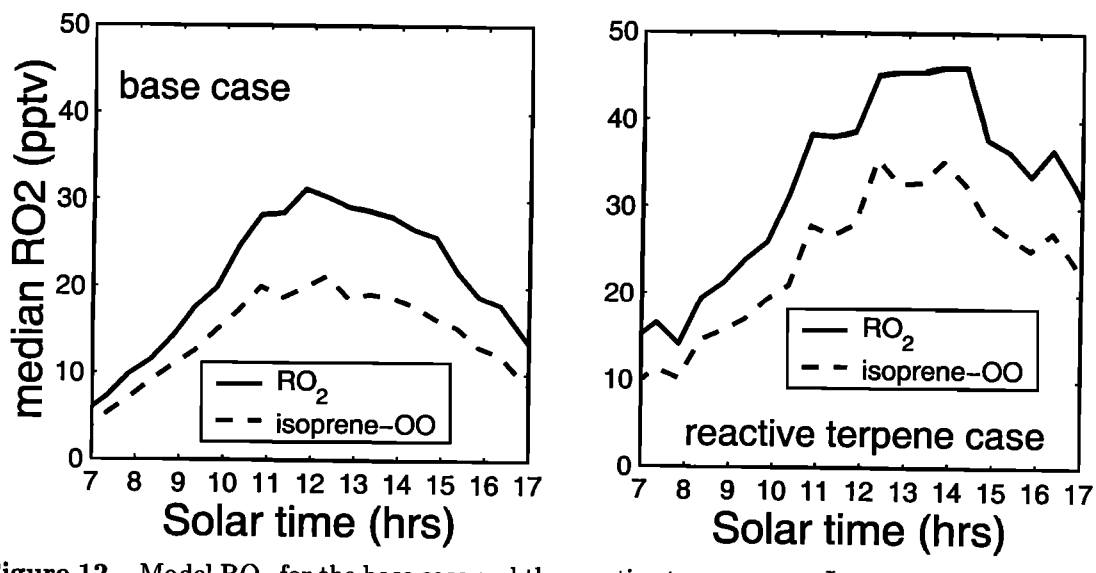

Figure 12. Model RO_2 for the base case and the reactive terpene case. Isoprene peroxy radicals make up approximately two-thirds of the total RO_2 in the base case, and over three-fourths of the total in the reactive terpene case.

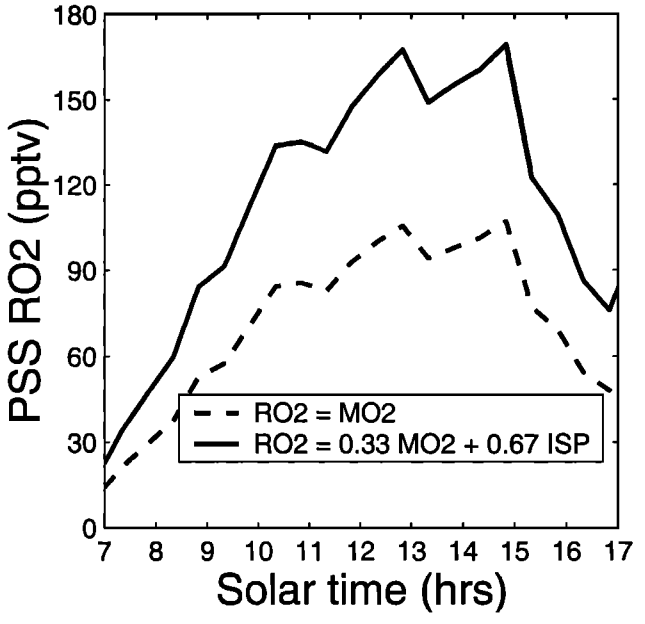

Figure 13. RO_2 as calculated by deviations from photostationary steady state. The dashed line uses the rate constant for MO2 + NO for all RO_2; the solid line uses the MO2 + NO rate constant for one-third of the RO_2, and the ISP + NO rate constant for the other two-thirds.

intensive is the only campaign of which the authors are aware in which OH, HO_2, and a full range of species important to HO_x were measured in a high BVOC, low NO environment; no opportunity is available to compare to other data sets from similar environments. However, OH and HO_2 are measured in identical fashion; in fact, for diagnostic purposes performed on an hourly basis, NO is injected upstream of the OH axis and HO_2 detected in the OH axis. This provides a check on the HO_2/OH ratio and the HO_2 calibration with respect to OH. The HO_2/OH ratios measured in this manner are essentially identical to the ratios measured during normal operation. Extensive calibrations were performed before, during, and after the campaign. While instrumental problems cannot be categorically ruled out, it is difficult to conjecture a scenario in which both the OH (but not HO_2) measurement and the measured HO_2/OH ratio are wrong.

We also cannot exclude the possibility of problems with one or more of the measurements constraining the model. The model is most sensitive to isoprene and NO; good agreement with the observations can be achieved by halving isoprene and doubling NO in the model. However, it is difficult to affect the model output sufficiently to match the observations by assuming inaccuracies in the measurements of species other than NO and isoprene. Isoprene was independently measured using three different techniques: all three measurements were in good agreement with each other [*Barket et al.*, this issue]. The NO measurement uses a standard, well-tested technique, and the instrument has performed well on several previous campaigns and intercomparisons [e.g. *Carroll et al.*, 1990; *Gregory et al.*, 1990; *Wang et al.*, 1996].

There is compelling evidence to indicate that species important to HO_x were present at PROPHET but were not measured. The elevated nighttime values of OH and the very low values of model OH compared to the measured OH indicate a nonphotolytic OH source, which we speculate may be the ozonolysis of a reactive terpene. The terpene measurements at PROPHET were not exhaustive; only those species initially thought to be significant were included. We are hopeful that the results from the PROPHET summer 1998 intensive will lead to further work in this area.

The present mechanisms used to model HO_x in an environment similar to PROPHET appear to suffer from two major shortcomings. The first is that it is almost certainly missing an OH source, which may be the ozonolysis of unmeasured terpenes. Even adding a source term nearly double the O^1D+ H_2O source, however, leaves the model OH at two thirds of the measured OH. Another candidate for a "missing source" is peroxides. The lifetime of peroxides in this environment is too long for a steady state approach to be appropriate, so peroxide concentrations in the model were fixed to levels comparable to measurements taken the previous summer. It is possible that peroxide concentrations during PROPHET 1998 were in actuality much higher than in the previous summer. A model run with peroxides constrained to 10 ppbv for hydrogen peroxide and for higher organic peroxides and 5 ppbv for methyl hydroperoxide increased the model OH by 11.6% over the base case model and HO_2 by 10.5% (when peroxides are explicitly calculated, median HOOH is 5.2 ppbv, CH_3OOH is 362 pptv, and ROOH is 6.9 ppbv, and the model OH and HO_2 each increase by 3% over the base case. These are purely gas phase calculations, with no peroxide depositional losses.) It is not likely that peroxides can make up for the model shortfall in OH or the discrepancy in the ratio. It should be noted, however, that the photochemistry of the larger hydroperoxides is poorly known and that the present model treatment of them may be far from complete. A more accurate treatment of these species may help close the discrepancy between model and observation.

The other shortcoming is that the cycling of HO_2 to OH is not described correctly. There is not enough NO for the available VOC to allow the model to maintain the observed HO_2/OH ratio. Increasing NO threefold in the model improves the agreement with the measurements: model OH in this scenario is within 10% of the measured OH, and model HO_2 is within 25% of the measured HO_2, although the model is still unable to capture the variability in the measurements. Evidently, the model only performs well when there is sufficient NO to ensure that the cycling from HO_2 to OH is fast relative to the HO_x sources and sinks. This implies that the chemical mechanism in this environment as it relates to

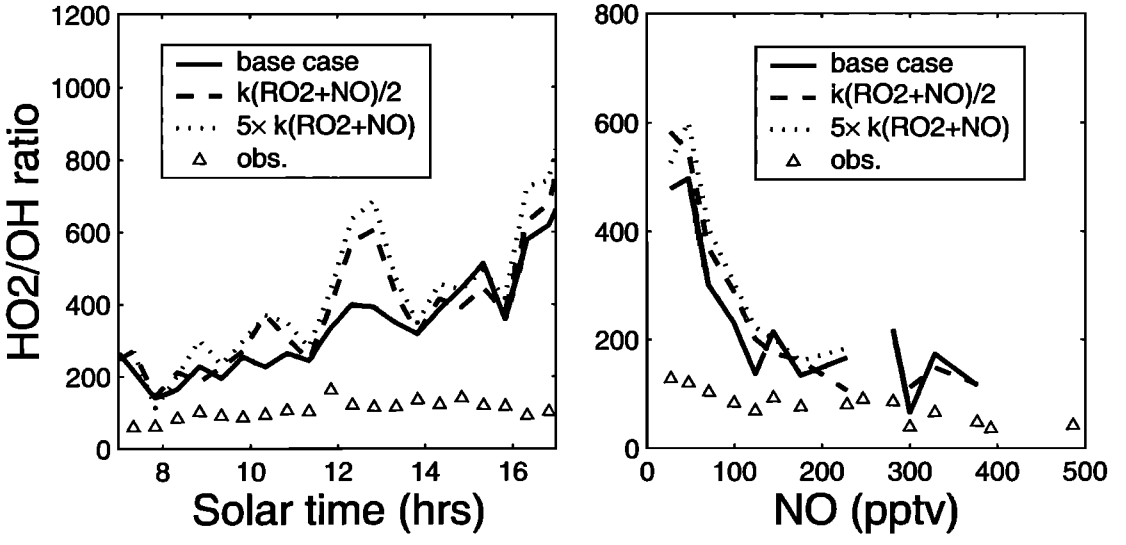

Figure 14. Diurnally averaged and NO-averaged median plots of the HO_2/OH ratio. Observed data are marked by symbols; model runs in the base case are marked by a solid line. The dashed line is the model run with the rate constants for higher-order RO_2 + NO set at half the literature value; the dotted line is the model run with k_{RO2+NO} set at 5 times the literature value. The measured OH and HO_2 were used as a common data basis in the calculation of the median values.

the cycling from HO_2 to OH is not correct. It may also imply a species or reaction scheme missing in the mechanism which can convert HO_2 to OH and which has a reduction potential similar to NO. (*Bohn and Zetzsch,* [1997] find a rate constant for the HO_2 + NO reaction to be ~ 20% higher than the Jet Propulsion Laboratory recommendation [*DeMore et al.,* 1997]. Using this rate constant in the model has little effect on the model prediction, with model OH increasing by less than 5% and model HO_2 decreasing by less than 3%.) There is also considerable uncertainty in the reaction rates of NO and higher-order (larger than CH_3OO) RO_2. Sensitivity runs to these reaction rates are shown in the dashed and dotted lines in Figures 5 and 14, with the dashed line showing the model run for RO_2 + NO rate constants set to half the literature values, and the dotted line showing the model run for RO_2 + NO rate constants set to 5 times the literature values. Lower values for these rate constants lead to lower HO_x, and vice-versa, although for both of these cases, the HO_2/OH ratio increases somewhat from the model base case. In all cases, the agreement is better at high NO than at low NO, although even at high NO, the model ratio is still more than twice the measured ratio. Similar uncertainties exist in the reaction rates of RO_2 with HO_2. Sensitivity to these rate constants (again, for RO_2 larger

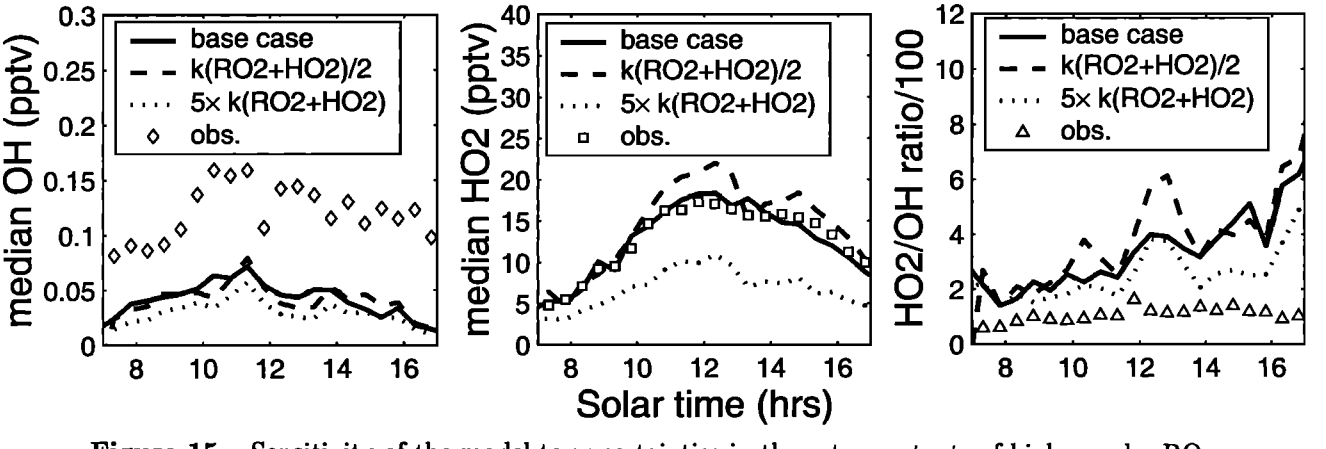

Figure 15. Sensitivity of the model to uncertainties in the rate constants of higher-order RO_2 and HO_2 are shown as diurnal medians of OH, HO_2, and the HO_2/OH ratio. Observations are marked by symbols; the model base case is marked by a solid line. The dashed line is the model run with the rate constants for higher-order RO_2 + HO_2 set at half the literature value; the dotted line is the model run with $k_{RO2+HO2}$ set at 5 times the literature value. The measured OH and HO_2 were used as a common data basis in the calculation of the median values.

than CH_3OO) is shown in Figure 15. HO_2 is quite sensitive to uncertainties in these rate constants; OH is relatively insensitive, even assuming that the RO_2 + NO (HO_2) rate constant is as much as 5 times the literature value. Some of the uncertainties in the modeling may be addressed by good (ideally speciated) measurements of RO_2, as well as more complete coverage of the terpenes. However, further laboratory work in the mechanism and kinetic parameters of BVOC oxidation in environments similar to PROPHET are required, as well.

It is possible that the model mechanism used here is inappropriate for the conditions found in PROPHET'98. Other possible mechanisms include *Carter and Atkinson,* [1996] and the unmodified RACM. It is, unfortunately, beyond the scope of this paper to provide a model intercomparison. However, a few words of justification may be in order. The Carter and Atkinson mechanism is more appropriate for high NO_x conditions, as the authors state clearly. Furthermore, it was tested against smog chamber experiments, where NO concentrations range from several tens of ppbv to ppmv. The mechanism used in this paper would probably not be appropriate for smog chamber studies under such high NO conditions. The standard RACM mechanism, on the other hand, is more appropriate for environments with greater anthropogenic contributions. The oxidation of isoprene and other biogenic VOC is not treated in specific detail, for example, whereas aromatic and nitrate radical chemistry are.

It is not surprising to find that the present modeling effort in this environment leaves something to be desired. The photochemistry of isoprene and other BVOCs is complex and not well characterized. Mechanisms and kinetic parameters generally come from smog chamber studies, where NO concentrations used are typically 3 to 5 orders of magnitude greater than NO concentrations found in PROPHET'98 (excepting the mechanism and kinetic data for the initial oxidation of isoprene). Many rate constants are not known and are estimated by similarity theory. In the present work we used data for the initial isoprene oxidation by OH and the isoprene peroxy radical reactions from an NO-free study [*Jenkin et al.,* 1998]; however, these data are from a single study, and the rest of the mechanism is derived from smog chamber experiments. Clearly, there is a need for more accurate elucidation of the mechanism and kinetic parameters of isoprene and BVOC oxidation. Beyond this, however, the implications at least for existing unconstrained modeling efforts are not clear. A case in point is *Staffelbach et al.,* [1997a, 1997b], a modeling effort in support of a field measurement campaign in southern Switzerland. The photochemical environment was similar to that for PROPHET, with somewhat higher levels of VOC, especially isoprene, and NO. Neither OH nor HO_2 were measured, so direct model to measurement comparisons are not possible. Two different models were used, however, one using the Harvard photochemical trajectory model with estimated VOC and NO_x emissions, the other a steady state point model constrained where possible to measured precursors. The trajectory model predicted an HO_2/OH ratio of $\sim$ 65, similar to if somewhat lower than the measured ratio at PROPHET, whereas the constrained point model predicted a ratio of over 350, comparable to the present work model ratio for the base (no reactive terpene) case. Examination of the discrepancy in detail showed that the isoprene concentration used in the trajectory model was several times lower than the measured isoprene and that the model NO was several times higher than the measured NO. The discrepancy was explained in part by a "surface gradient effect," since the measurements were taken at 3 m elevation above the ground, and the lowest layer in the model was from 0 to 40 m. The canopy height of the surrounding forest was not mentioned. Similarly, *Volz-Thomas and Kolahgar,* [2000] found that a trajectory model used to model OH at the Schauinsland Ozone Precursor Experiment (SLOPE96) estimated OH concentrations about twice those calculated by a constrained zero-dimensional (0-d) point model. As in the case of Staffelbach, neither OH nor HO_2 were measured during SLOPE96. At PROPHET 1998, the same issue arose in a one-dimensional (1-D) trajectory model using BEIS2 emissions and isoprene oxidation from Carter and Atkinson [S. Sillman, unpublished data, 2001]: the model agreed quite well with the measurements for OH and HO_2 when the model used area-wide (20x20 km resolution) emission estimates for isoprene but significantly underestimated OH and overestimated the HO_2/OH ratio when using isoprene emissions based on specific forested locations. It is quite possible that existing unconstrained model efforts in environments similar to the PROPHET environment fortuitously yield reasonable results for the wrong reasons, particularly if the models relied on relatively large-scale emission estimates.

The constrained point models used in the TOHPE, LAFRE, and EASE96 campaigns all predicted higher levels of OH and HO_2 than were actually measured. This is not necessarily inconsistent with the present constrained model effort: the photochemical conditions for each campaign were quite different. LAFRE conditions were dominated by the very high anthropogenic loadings characteristic of the Los Angeles basin, whereas the conditions at EASE96 may be characterized as primarily marine boundary layer air. PROPHET is photochemically most similar to the clean conditions (westerly flow) at TOHPE; however, much more isoprene was measured at PROPHET than at TOHPE (several ppbv versus 100-300 pptv). Unlike the case at PROPHET, the oxidation of isoprene did not dominate OH loss at TOHPE [*Goldan et al.,* [1997]; in fact, the most important contributions to OH loss were CO followed by methane for low-NO_x conditions, and NO_2 followed by CO for high-NO_x conditions [*McKeen et al.,* [1997]. *Stevens et al.,* [1997] note that the HO_2/OH

ratios calculated by a constrained steady-state model agreed well with the measured ratios at high NO_x, but were 3-4 times higher than the measured ratios at low NO_x. While the differing photochemical conditions at TOHPE and PROPHET preclude genuine comparison, and while the models for TOHPE overpredicted OH and HO_2 whereas that for PROPHET underpredicted OH, it is nonetheless interesting that both model efforts exhibit similar behavior in the agreement with measurement with respect to NO_x.

Acknowledgments. The authors would like to thank the National Science Foundation's Atmospheric Chemistry program and Anne-Marie Schmoltner, whose support made this work possible with grants ATM-9628059 and ATM-9628059 Amendment 001. Sandy Sillman, Geoffrey Tyndall, Hartwig Harder, and Monica Martinez provided useful advice and many helpful discussions. The authors would also like to thank everyone involved in PROPHET 1998 for the use of data, as well as the University of Michigan Biological Station for help and support.

References

Atkinson, R., Gas-phase tropospheric chemistry of volatile organic compounds: 1. Alkanes and alkenes, *J. Phys. Chem. Ref. Data*, *26*(2), 215-290, 1997.

Barket, D., Jr., et al., Intercomparison of automated methodologies for determination of ambient isoprene during the PROPHET 1998 summer campaign, *J. Geophys. Res.*, this issue.

Bohn, B., and C. Zetzsch, Rate constants of HO_2 + NO covering atmospheric conditions. 1. HO_2 formed by OH + H_2O_2, *J. Phys. Chem. A*, *101*, 1488-1493, 1997.

Brune, W. H., et al., Airborne *in-situ* OH and HO_2 observations in the cloud-free troposphere and lower stratosphere during SUCCESS, *Geophys. Res. Lett.*, *25*, 1701-1704, 1998.

Cantrell, C. A., R. E. Shetter, J. B. Calvert, F. L. Eisele, E. Williams, K. Baumann, W. H. Brune, P. S. Stevens, and J. H. Mather, Peroxy radicals from photostationary state deviations and steady state calculations during the Tropospheric OH Photochemistry Experiment at Idaho Hill, Colorado, 1993, *J. Geophys. Res.*, *102*, 6369-6378, 1997.

Carroll, M. A., et al., Aircraft measurements of NO_x over the eastern Pacific and continental United States and implications for ozone production, *J. Geophys. Res.*, *95*, 10,205-10,233, 1990.

Carroll, M. A., P. B. Shepson, and S. B. Bertman, Overview of the Program for Research on Oxidants: Photochemistry, Emissions, and Transport (PROPHET) summer 1998 measurements intensive, *J. Geophys. Res.*, this issue.

Carslaw, N., D. J. Creasey, D. E. Heard, A. C. Lewis, J. B. McQuaid, M. J. Pilling, P. S. Monks, B. J. Bandy, and S. A. Penkett, Modeling OH, HO_2, and RO_2 radicals in the marine boundary layer, 1, Model construction and comparison with field measurements, *J. Geophys. Res.*, *104*, 30,241-30,255, 1999a.

Carslaw, N., P. J. Jacobs, and M. J. Pilling, Modeling OH, HO_2, and RO_2 radicals in the marine boundary layer, 2, Mechanism reduction and uncertainty analysis, *J. Geophys. Res.*, *104*, 30,257-30,273, 1999b.

Carter, W. P. L., and R. Atkinson, Development and evaluation of a detailed mechanism for the atmospheric reactions of isoprene and NO_x, *Int. J. Chem. Kinet.*, *28*, 497-530, 1996.

Cooper, O. R., J. L. Moody, T. Thornberry, M. Town, and M. A. Carroll, PROPHET 1998 meteorological overview and air mass classification, *J. Geophys. Res.*, this issue.

DeMore, W. B., S. P. Sander, D. M. Golden, R. F. Hampson,, M. J. Kurylo, C. J. Howard, R. Ravishankara, C. E. Kolb, and M. J. Molina, Chemical kinetics and photochemical data for use in stratospheric modeling, in Evaluation 12, *JPL Publ. 97-4*,, Jet Propul. Lab., Pasadena, Calif., 1997.

Dransfield, T. J., K. K. Perkins, N. M. Donahue, J. G. Anderson, M. M. Sprengnether, and K. L. Demerjian, Temperature and pressure dependent kinetics of the gas-phase reaction of the hydroxyl radical with nitrogen dioxide, *Geophys. Res. Lett.*, , *26*(6), 687-690, 1999.

Faloona, I., et al., Nighttime observations of anomalously high levels of hydroxyl radicals above a deciduous forest canopy, *J. Geophys. Res.*, this issue.

George, L. A., T. M. Hard, and R. J. O'Brien, Measurement of free radicals OH and HO_2 in Los Angeles smog, *J. Geophys. Res.*, *104*, 11,643-11,655, 1999.

Gregory, G. L., at al., An intercomparison of airborne nitrogen dioxide instruments, *J. Geophys. Res.*, *95*, 10,103-10,128, 1990.

Hard, T. M., R. J. O'Brien, C. Y. Chan, and A. A. Mehrabzadeh, Tropospheric free radical determination by FAGE, *Environ. Sci. Technol.*, *18*, 768, 1984.

Jenkin, M. E., A. A. Boyd, and R. Lesclaux, Peroxy radical kinetics resulting from the OH- initiated oxidation of 1,3-butadiene, 2,3-dimethyl-1,3-butadiene and isoprene, *J. Atmos. Chem.*, *29*, 267-298, 1998.

Levy, H., Photochemistry of the lower troposphere, *Planet. Space Sci.*, *20*, 919-935, 1972.

Logan, J. A., M. J. Prather, S. C. Wofsy, and M. B. McElroy, Tropospheric chemistry, a global perspective, *J. Geophys. Res.*, *86*, 7210-7254, 1981.

Madronich, S., Intercomparison of NO_2 photodissociation and U.V. radiometer measurements, *Atmos. Environ.*, *21*(3), 569-578, 1987a.

Madronich, S., Photodissociation in the atmosphere, 1, Actinic flux and the effects of ground reflection and clouds, *J. Geophys. Res.*, *92*, 9740-9752, 1987b.

Makar, P. A., J. D. Fuentes, D. Wang, R. M. Staebler, and H. A. Wiebe, Chemical processing of biogenic hydrocarbons within and above a temperate deciduous forest, *J. Geophys. Res.*, *104*, 3581-3603, 1999.

McKeen, S. A., et al., Photochemical modeling of hydroxyl and its relationship to other species during the Tropospheric OH Photochemistry Experiment, *J. Geophys. Res.*, *102*, 6467-6495, 1997.

Mount, G. H., and E. J. Williams, An overview of the Tropospheric OH Photochemistry Experiment, *J. Geophys. Res.*, *102*, 6171-6186, 1997.

Mount, G. H., J. W. Brault, P. V. Johnston, E. Marovich, R. O. Jakoubek, C. J. Volpe, J. Harder, and J. Olson, Measurement of tropospheric OH by long-path laser absorption at Fritz Peak Observatory, Colorado, during the OH Photochemistry Experiment, fall 1993, *J. Geophys. Res.*, *102*, 6393-6414, 1997.

Paulson, S. E., R. C. Flagan, and J. H. Seinfeld, Atmospheric photooxidation of isoprene part I, The hydroxyl radical and ground state atomic oxygen reactions, *Int. J. Chem. Kinet.*, *24*, 79-101, 1992.

Staffelbach, T., et al., Photochemical oxidant formation over southern Switzerland, 1. Resuts from summer 1994, *J. Geophys. Res.*, *102*, 23345-23362, 1997a.

Staffelbach, T., A. Neftel, and L. W. Horowitz, Photo-

chemical oxidant formation over southern Switzerland, 2. Model results, *J. Geophys. Res., 102,* 23363-23373, 1997b.

Stevens, P. S., J. H. Mather, and W. H. Brune, Measurement of OH and HO_2 by laser- induced fluorescence at low pressure, *J. Geophys. Res., 99,* 3542-3557, 1994.

Stevens, P. S., et al., HO_2/OH and RO_2/HO_2 ratios during the Troposheric OH Photochemistry Experiment: Measurement and theory, *J. Geophys. Res., 102,* 6379-6392, 1997.

Stockwell, W. R., F. Kirchner, M. Kuhn, and S. Seefeld, A new mechanism for regional atmospheric chemistry modeling, *J. Geophys. Res., 102,* 25,847-25,879, 1997.

Sumner, A. L., et al., A study of formaldehyde chemistry above a forest canopy, *J. Geophys. Res.,* this issue.

Tanner, D. J., A. Jefferson, and F. L. Eisele, Selected ion chemical ionization mass spectrometric measurement of OH, *J. Geophys. Res., 102,* 6415-6426, 1997.

Thornberry, T. D., et al., Observations of reactive oxidized nitrogen and speciation of NO_y during the PROPHET 1998 summer intensive, *J. Geophys. Res.,* this issue.

Volz-Thomas, A., and B. Kolahgar, On the budget of hydroxyl radicals at Schauinsland during the Schauinsland Ozone Precursor Experiment (SLOPE96), *J. Geophys. Res., 105,* 1611-1622, 2000.

Wang, T., M. A. Carroll, G. M. Albercook, K. R. Owens, K. A. Duderstadt, A. N. Markevitch, D. D. Parrish, J. S. Holloway, G. Forbes, J. Ogren, Ground-based measurements of NO_x and total reactive oxidized nitrogen (NO_y) at Sable Island, Nova Scotia, during the NARE 1993 intensive, *J. Geophys. Res., 101,* 28991-29004, 1996.

Zimmerman, J. and D. Poppe, A supplement for the RADM2 chemical mechanism: The photooxidation of isoprene, *Atmos. Environ., 30*(8), 1225-1269, 1996.

E. Apel and I. Faloona, Atmospheric Chemistry Division, National Center for Atmospheric Research, Boulder, CO, 80303.

W. Brune and J. B. Simpas, Department of Meteorology, The Pennsylvania State University, University Park, PA 16802. (email: brune@essc.psu.edu)

M. A. Carroll and T. Thornberry, Atmospheric, Oceanic, and Space Sciences, The University of Michigan, Ann Arbor, MI 48109.

T. L. Couch, P. B. Shepson, and A. L. Sumner, Department of Chemistry, Purdue University, West Lafayette, IN 47907.

D. Riemer, Rosenstiel School of Marine and Atmospheric Science, The University of Miami, Miami, FL 33149.

W. Stockwell, Western Regional Climate Center, Desert Research Institute, Reno, NV 89512.

D. Tan, School of Earth and Atmospheric Sciences, Georgia Institute of Technology, Atlanta, GA 30332. (email: dtan@eas.gatech.edu)

(Received March 31, 2000; revised December 15, 2000; accepted December 26, 2000.)